Dissertations, Theses, and Masters Projects   Theses, Dissertations, & Master Projects

2013

Holocene Sedimentation on the Lanyang Plain and Adjacent Continental Shelf, Northwestern Taiwan

Chia-Yu Wu
College of William and Mary - Virginia Institute of Marine Science

Follow this and additional works at: https://scholarworks.wm.edu/etd

Part of the Geology Commons, and the Oceanography Commons

Holocene Sedimentation on the Lanyang Plain and Adjacent Continental Shelf,

Northeastern Taiwan

———————————

A Thesis

Presented to

The Faculty of the School of Marine Science

The College of William and Mary in Virginia

In Partial Fulfillment

of the Requirements for the Degree of

Master of Science

———————————

By

Chia-Yu Wu

APPROVAL SHEET

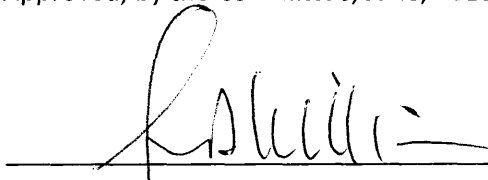This thesis is submitted in partial fulfillment of

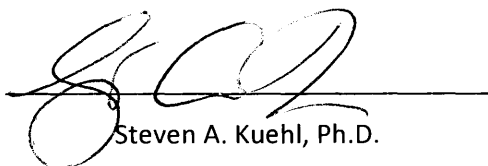the requirements for the degree of

Master of Science

Chia-Yu Wu

Approved, by the Committee, June, 2013

John D. Milliman, Ph.D.
Committee Chairman/ Advisor

Steven A. Kuehl, Ph.D.
Committee Co-Chairman /Co-Advisor

Mark J. Brush, Ph.D.

Harry V. Wang, Ph.D.

Char-Shine Liu, Ph.D.
National Taiwan University
Taipei, Taiwan

TABLE OF CONTENT

LIST OF FIGURES

LIST OF TABLES

Acknowledgements

I'd really want to thanks to many people who guided me at VIMS, especially both of my advisors Dr. John Milliman and Dr. Steve Kuehl. Without your scientific guidance, I cannot finish this research by myself. I also gratefully acknowledge Drs. Mark Brush, Harry Wang and Char-Shine Liu, for giving me many suggestions and discussion. Specially, thanks to Dr. Char-Shine Liu to provide me many seismic data; Dr. Meng-Long Hsieh and the Central geological survey in Taiwan to provide me core data.

I would also thank to many of my good friends at VIMS, especially Wes, Jennifer and Julia who help me on many things. Also, thanks to lots of Chinese fellows such as Yonjing who help on daily life stuff.

The last but not the least, I want to thanks to my dear family and my dear girlfriend Tianwu, without your supporting and understanding, I cannot finish this thesis.

Abstract

The Lanyang Plain, along the northeastern Taiwan orogen, provides an excellent example of the tectonic and climatic controls on erosion and subsequent riverine sediment supply to the coastal ocean and deep sea. 12 deep borings on the Lanyang Plain and 2 long cores in Southern Okinawa Trough (MD12403, ODP1202), together with high-resolution seismic data on Ilan Shelf, provide a good record of the depositional history during Holocene, in both on-land and offshore areas. Based on these data, we find the sediment thickness reaches 216 m in Lanyang Plain, and the average sediment rate is estimated to be 3.6 Mt/yr - 5 Mt/yr in both the Lanyang Plain and the Ilan shelf. This value is higher than previous estimation of 2.6 Mt/yr by Kao and Milliman (2008).

We have divided on-land sedimentation rates over different periods (0-4 ka BP, 4-8 ka BP, and 8-12 ka BP) to document variations in Holocene sedimentation in response to event-enhanced and/or accommodation-space change. We find particularly high accumulation rates at 8-12 ka BP. Higher sedimentation rates noted in 2 offshore cores occurred at the same time. Together, this suggests greater sedimentation during this period, which we suggest may be related to the regional intensification of the southwest (summer) monsoon in Southern Asia, perhaps reflected by increased typhoon activity. Scrutinizing data from other previous studies, this event seems to have been characterized by higher sediment accumulation throughout Taiwan.

Holocene Sedimentation on the Lanyang Plain and Adjacent Continental Shelf, Northeastern

Taiwan

1

1. Introduction

The major sediment source for most offshore depositional systems is fluvial. Among the major rivers in the world, the greatest amounts of global fluvial sediments are delivered by Asian rivers (Milliman and Syvitski, 1992; Liu et. al., 1998; Xu et al., 2012), such as the Yangtze River and Ganges–Brahmaputra River. Milliman and Syvitski (1992) also indicated the importance of small mountainous rivers on tectonically active islands, such as Taiwan, to the global sediment flux into the oceans. Under these tectonic settings, the flux of fluvial sediment can be significantly affected by the complex interplay between environment (e.g., climate, tectonics, and hurricane) and human activities (Milliman and Syvitski., 1992; Syvitski and Milliman., 2007; Liu et al., 1998). With active tectonic movement, high relief and steep gradients, as well as heavy rainfall and frequent typhoons, Taiwan rivers, for example, have some of the highest sediment yields in the world (Li, 1976; Milliman and Meade, 1983; Kao et al., 2005a; Milliman and Farnsworth, 2011). Catastrophic earthquake or typhoon events can also enhance high sediment discharge. For instance, the sediment concentrations in rivers were 4 times higher than decadal background values after the Chi-Chi earthquake in Taiwan (September, 21, 1999; Dadson et al., 2004). Similarly, Typhoon Morakot (August 2009) triggered more than 12,000 landslides (Wu et al., 2011) in Southern Taiwan, resulting in catastrophic sediment discharge (Wu et al., 2011; Hsieh et al., 2012; Tsou et al., 2010).

While the above examples show how environmental factors (e.g., typhoons and earthquakes) can strongly affect the sediment discharge over periods of historical river monitoring, especially in areas where active tectonic and subtropical climates interface, such

as Taiwan (Dadson et al., 2004), longer-term changes resulting from variations in climate

patters can be similarly dramatic. For example, millennial-scale changes in the Asian summer

monsoon have been documented from numerous studies (e.g., Altabet et al., 2002; Clemens

et al., 1991), and these have been shown to have been translated into major changes in

landscape evolution and sediment yield in Asian regions. For example, Goodbred and Kuehl

(2000) demonstrated a two-fold increase in sediment output from the Ganges–Brahmaputra

River between 11 ka BP (thousand years before present) and 7 ka BP, which correlated to the

post-Late Glacial Maximum (post-LGM) intensification of Asian summer monsoon. Other

studies in the northwest Himalayas suggest an even greater increase (5-fold) in sediment

yield during this same period (Bookhagen et al., 2005). When viewed over Later Quaternary

time scales, changing climate patterns clearly can therefore have a dominant influence on

river sediment discharge.

In addition to natural change, human perturbations (e.g., deforestation, agricultural

activity, urbanization) are considered to be an important factor that has contributed to the

increase the sediment flux in modern period (Syvitski et al., 2005). Syvitski and Milliman

(2007) suggested that globally, anthropogenic factors can account for 16% of sediment loads,

but locally human activities can have a greater impact on the sediment discharge in highly

erosive watersheds. For example, sediment loads of the Lanyang River in northeastern

Taiwan increased dramatically after several major short-lived disturbances, such as road

construction and typhoon events (Kao and Liu, 2001).

The first step to distinguish the different factors that affect the variations of sediment

accumulation is to calculate sedimentation rates over different time scales. However, it is

difficult to quantify the sediment accumulation patterns due to the lack of long-term river

monitoring as well as that few rivers discharge into enclosed or semi-enclosed basins into

which all or most of the sediment accumulates. The Lanyang River is therefore unusual

because not only does it have a relatively long-term database but it also discharges into a

semi-enclosed basin, Southwestern Okinawa Trough (SOT) (Fig. 1).

In addition to having a relatively long database (1949-present), the Taiwan Central

Geology Survey (CGS), Ministry of Economic Affairs, has rich archive of radiocarbon ages (^{14}C)

from 16 groundwater cores across the Lanyang (flood) Plain. From these 100-300 m-long

cores, there are more than 90 ^{14}C dates, most of which give dates <15 ka BP. Moreover,

during the cruise of OR2-1313 (Ocean Research 2), some critical seismic profiles were

gathered on the Ilan Shelf (Fig. 2), and provide good constraint of sediment deposition

pattern in the region. By combining the on-land core dates and the seismic profiles, we can

investigate sedimentation and dispersion across the Lanyang Plain and the Ilan Shelf. These

data provide excellent on-land and offshore sediment deposition records during Holocene

both temporally and spatially.

In addition, two long cores (>20 m) in Southwestern Okinawa Trough (SOT) region have

more than 20 ^{14}C dates: one core from the Ocean Drilling Program site (ODP 1202) (Wei et al.

2005), and the other Marion Dufresne core (MD12403) (Kao et al. 2005b, 2008) (Fig. 2).

These offshore cores can help show if Lanyang-derived sediment has escaped to the deep

ocean basin and if this escape coincides with any possible climate and/or tectonic change.

Calculating the deposition rates of fluvial and near-shore sediments allows us to delineate

the variation in sediment erosion and deposition, as well as to compare the role of environmental and/or human impact on sediment flux. The Lanyang River watershed and Ilan shelf data are sufficiently long and extensive to allow us to delineate the effect of shifts in sediment fluxes due to different factors (climatic, tectonic or anthropogenic). The purpose of this study therefore is to estimate the sediment flux from the Lanyang River throughout the Holocene in an attempt to understand how sediment flux responds to different natural and/or various human perturbations.
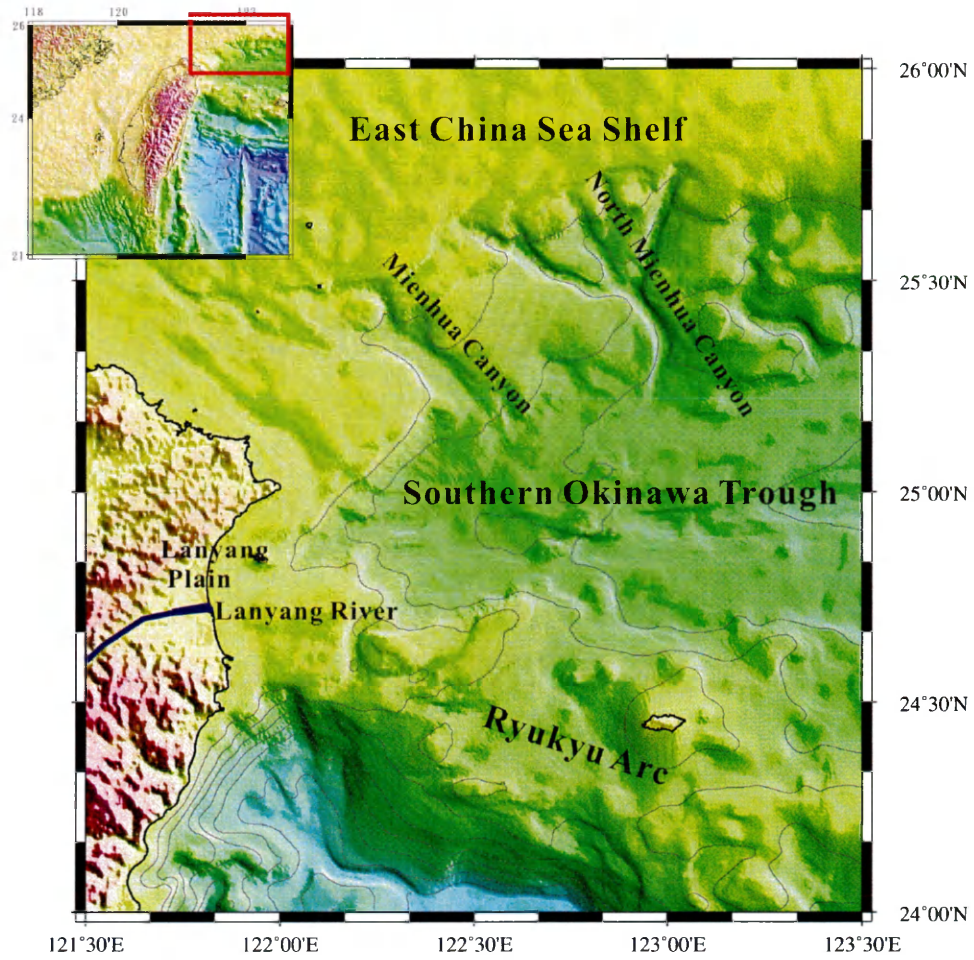
Fig. 1. Location and physiographic features of our study area. The black lines represent the contours of 500m interval.
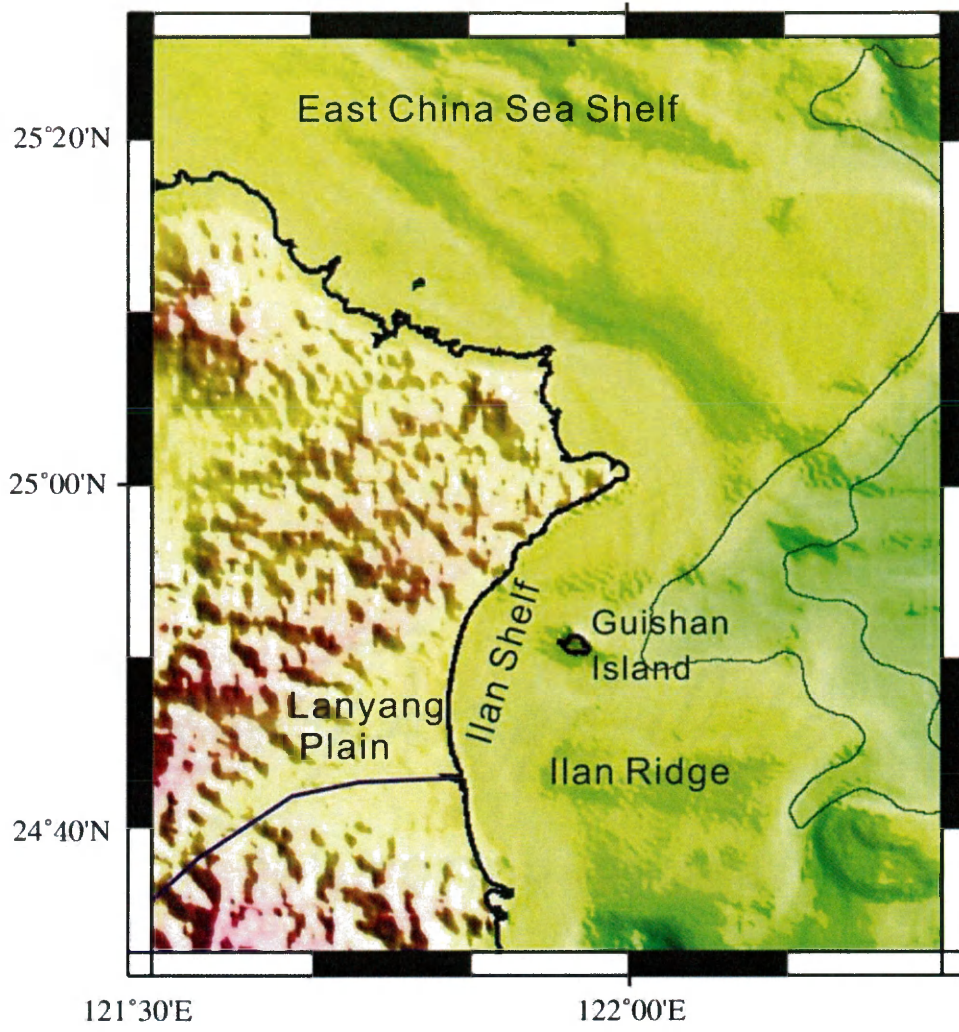
Fig. 2. Near-shore location and physiographic features of our study area.

2. Study area

The study area includes the Lanyang Plain, Ilan shelf, and southernmost part of SOT (Fig. 1 & 2). The SOT is a back-arc basin in the collision zone between the Philippine Sea plate and the Eurasian plate. Its progressive westward propagation is splitting the mountain ranges surrounding the Lanyang Plain (Fig. 3) (Suppe, 1984; Teng, 1996), forming a triangular basin that is extended by normal faults (Lee et al., 1980; Sibuet et al., 1998; Shyu et al. 2005), also creating a volcanic island- Gueshan Island (Chen et al., 2001). The Lanyang Plain has a 2-cm/year subsidence rate (Liu et al., 1995), which provides large accommodation space to store the sediment output from Lanyang River.

The Lanyang River originates in Nan-Hu Mountain (3535 m above sea level) with a mean 5% gradient. The length of Lanyang River is 73 km with drainage area of 980 km^2. Average annual precipitation in the Lanyang watershed is about 3250 mm/yr, rainfall being most abundant during the southwest (summer) Asian monsoon season, particularly during typhoons. With steep gradients and abundant rainfall, Lanyang River has one of highest sediment yields in the world (Milliman and Farnsworth, 2011), with present-day annual sediment load of about 8 -17 Mt/year (Jen and Kao, 2002; Dadson et al., 2003; Milliman and Kao, 2005; Huh et al., 2006). Prior to road construction in the early 1960s, however, sediment discharge was <3 Mt/yr (Kao and Liu, 2001; Syvitski and Milliman, 2007).

The bulk of the river-derived sediment is deposited on the Lanyang Plain and in the adjacent Ilan Shelf region and eventually to the SOT (Kao and Liu, 2001), with total sediment thickness on the Lanyang Plain reaching more than 1200m in depth (Chiang,

1976).

The Ilan shelf is a narrow continental shelf varying in width between ~2 to 10 km. The shelf represents a seaward continuation of the Lanyang Plain, with narrowing at the north and south ends and relatively smooth and flat bottom (Yu and Hong, 1992; Yu and Song, 2000). As with the Lanyang Plain, Ilan Shelf is covered by late Quaternary sediment derived from the Lanyang River system (Hong et al. 2000). One important physiographic uplift unit on the shelf is the Ilan Ridge, which is located in the southern Ilan shelf and faces the Lanyang River; it contains steep slopes and has a seamount submarine channels. At present the Ilan Ridge can be considered as an extension of the Ryukyu Island Arc, but the actual mechanism of formation is not clear (Hong et al., 2000) (Fig. 2).
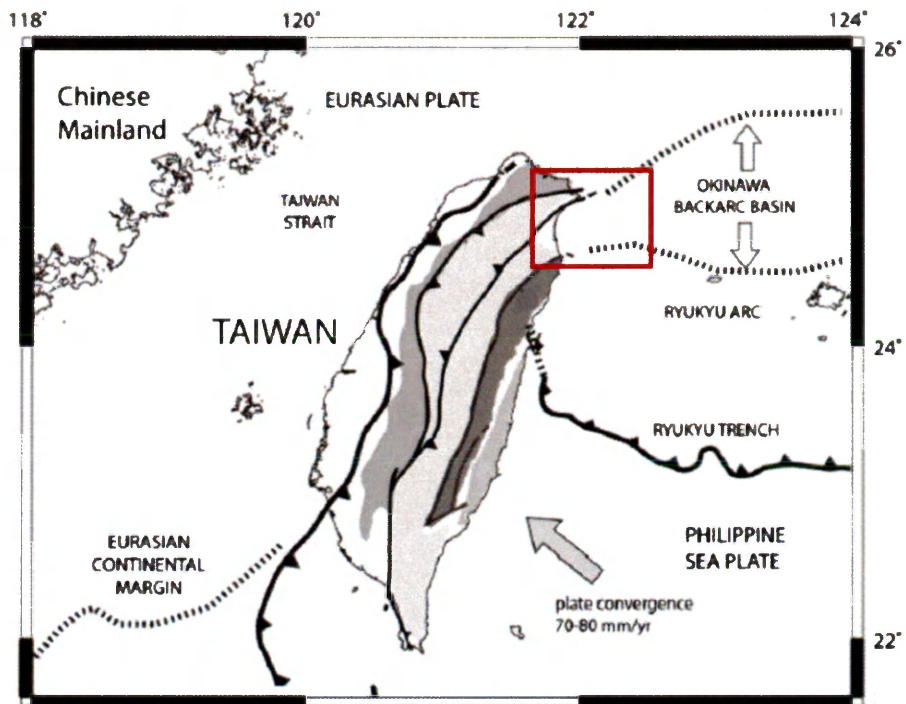
Fig. 3. The tectonic setting in Taiwan, our study area is outlined in red. The Philippine Sea Plate converges with the Eurasian Plate at a rate of 70-80mm/yr, and induces the back-arc splitting in SOT (Modified from Gourley et al., 2007).

3. Methods

The sediment volume calculation assumes the sediment deposit is wedge-shaped on the delta (coastal plain) and adjacent continental shelf (Fig. 4). In order to calculate sediment accumulation in our study area, data from 12 on-land cores on the Lanyang Plain and 4 high-resolution seismic profiles were combined. More than 90 ^{14}C dates provide a detailed record of the Holocene depositional history of Lanyang Plain area. These dates were extrapolated offshore to seismic reflection profiles taken on the shelf. Collectively, these data help us to generate the isopach map during Holocene. In addition, 2 long cores from the adjacent offshore SOT (MD12403, ODP1202) help us envision possible seaward sediment escape from the Lanyang Plain and shelf (Fig. 5).

3.1 Core description

3.1.1 On-land cores

The Central Geological Survey drilled 16 cores in the Lanyang plain, with 8 cores each north and south of the Lanyang River (Fig. 6). Chen et al. (2000) described the character of these cores, including their grain size, sedimentary structures and dating data. The number of radiocarbon dates from each core ranges from 0-12. In order to present more robust results, we excluded the cores with less than 5 dates from the analysis, with a single exception: core SS (blue in Fig. 6) located upstream near the adjacent mountains, contains only 3 dates, but to establish a precise sediment distribution pattern for Holocene isopach in the upper plain, dates from this core were used to help construct the isopach map. All of

these selected cores were drilled to a depth over 150 m, and the deepest dates reached

over 20 ka BP. Collectively these data provided us the basis for establishing chronological

framework of the Holocene sequence (~12 ka BP).

The dating material included shells, peat, wood, root, plant fragment and organic mud.

We excluded dates from organic mud because they presumably include fossil organic carbon

that would result in a very old ^{14}C dates. One of the dates in WY core shows 3833 yr BP in

calibrated age, which is younger than the above one (Calibrated as 5516 yr BP), and resulted

in negative sediment rate (-1.23 cm/yr) (Marked as red number in Table 1)., Accordingly, this

date was not used.

3.1.2 Offshore cores

As previously mentioned, two offshore cores (ODP1202, MD12403) are used to

investigate the potential for sediment escape offshore. Core ODP1202, located along the

southern slope of the Southern Okinawa Trough (24°48'N, 122°30'E; water depth 1274 m),

was collected to gain a record of late Quaternary variations of the Kuroshio (Wei et al., 2005).

There are four holes in total drilled at ODP1202 (ODP1202A to D), with 11 radiocarbon from

ODP1202B (total core length 140.5 m; Wei et al., 2005) used in this study.

Piston core MD012403 was taken in 2001 from the R/V Marion Dufresne at 25°16.98'N,

123°09.60' E in the Southern Okinawa Trough, water depth 1420 m, during the International

Marine Global Changes Study program (IMAGES VII) (Bassinot et al., 2002; Kao et al., 2005b,

2008). Total core length was 36 m, penetrating down to the Last Glacial Maximum (LGM)

layer. Kao et al. (2005, 2008) reported 13 radiocarbon dates obtained from 12 depths in the

core.

All radiocarbon dates were obtained at selected intervals using >250 um planktonic foraminiferà *Globigerinoides ruber* and *Orbulina univers.* These radiocarbon dates and sediment accumulation rates of these offshore cores are compiled in Table 2. One of the dates in MD012403 (calibrated age 10,373 BP) showed too close to the above age (calibrated age 10,372 BP) (Table 2), resulting in a 4 orders of magnitude increase in sediment accumulation rate (190 vs. ~0.05 to 0.4cm/yr). We therefore omitted this date from our calculations.

3.2 Radiocarbon dating

All the published ^{14}C dates in this study were obtained in New Zealand, USA and France, using the AMS (Accelerator Mass Spectrometer) radiocarbon dating analytical method, allowing as little as 1-2 milligrams of organic carbon to be dated. In total there are 91 dates from the on-land cores and 24 dates from offshore cores. Collectively these data provide a basis for establishing chronological framework of the core sequences and Holocene sedimentation rates. All ^{14}C dates ages converted to calendar years (before AD1950) using CALIB 6.1 (Stuiver et al., 1998). These calibrated ages may differ slightly with the reported calibrated dates because of different versions of calibration software. Sediment accumulation rates were calculated by dividing the difference of core depth by upper and lower dates (Fig. 7 shows the core sample). Tables 1 and 2 show all the results.

3.3 High-resolution seismic data

The distribution and configuration of sediment from the on-land area to the shelf area can be defined by high-resolution seismic profiles. Using these data, we can extend the sediment on-land isopach to the shelf break (100-125m of water depth). There are 4 critical high-resolution seismic profiles gathered from the cruise OR2-1313 (Ocean Researcher 2) during September 2005 (See Fig. 5 for profile tracks).

The high-resolution seismic data were collected using a 40-in^{3}GI (generator and injector) gun fired at 5-second intervals. The receiver was a 12- channel hydrophone streamer. The recording depth in the GI gun seismic system is <1 second of two-way travel time. All seismic profiles were processed with ProMAX and SIOSEIS programs. The data processing procedures included trace editing, de-convolution, multiple attenuation, stacking, band-pass filter and spiking noise removal. All data processing was done by Prof. Char-Shine Liu's group at Institute of Oceanography, National Taiwan University. Note that all profiles have obvious multiples (Fig. 5 and 6).

One E-W seismic profile from Line 1 (Fig. 8a) can be directly linked to the CA core, with a ~3 km gap between the two (red dash line in Fig. 6). The dates from CA core, however, suggest the unconformity of the Holocene boundary (12 ka BP) across the shelf area. Using Line 1, the other seismic profiles (Fig. 8b, 9) can be similarly interpreted, such that the northern, eastern and southern edges of the Holocene delta can be constrained. Using a two-way travel time (TWTT), we can multiply by the P-wave velocity in the sea water (1500m/s) and divide by 2 to represent the sediment thickness.

3.4 ArcGIS analysis

To draw the isopach map on Lanyang Plain, we used the on-land cores radiocarbon dates with the Kriging interpolating method of ArcGIS software. The Kriging method assumes that the distance between the points reflects a spatial correlation, the interpolating value not biased by the surrounding values (ArcGIS handbook). The Kriging method is broadly used in different research fields, such as soil and geological science, and seems to be the most appropriate way to illustrate the variation of the sediment thickness on Lanyang Plain.

We used the default function of ordinary Kriging method (spherical semivariogram model and variable search radius) provided by ArcGIS. By using the kriging method, different isopach maps could be generated by using different data sets. The on-land Holocene isopach map was created by using the dates from on-land cores (both red and blue in Fig. 6). The Holocene isopachs of both the Lanyang Plain and Ilan shelf are generated by using the both of on-land dates along with the reflection depths from seismic profiles. In order to illuminate varying sediment patterns throughout the Holocene, we also divided the on-land core dates (red triangles in Fig. 6) into 3 time series: 0-4 ka BP, 4-8 ka BP and 8-12ka BP. These isopach maps help us to delineate any temporal changes in sedimentation.
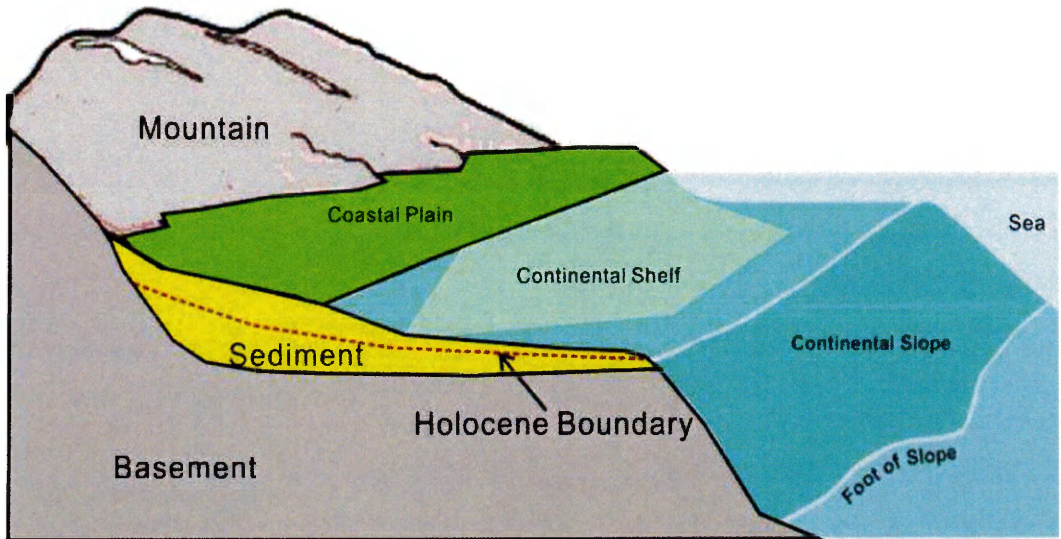
Fig. 4. Conceptual visualization of sediment thickness calculation. The yellow layer between the surface and Holocene boundary is the sediment thickness that has been calculated in the study.
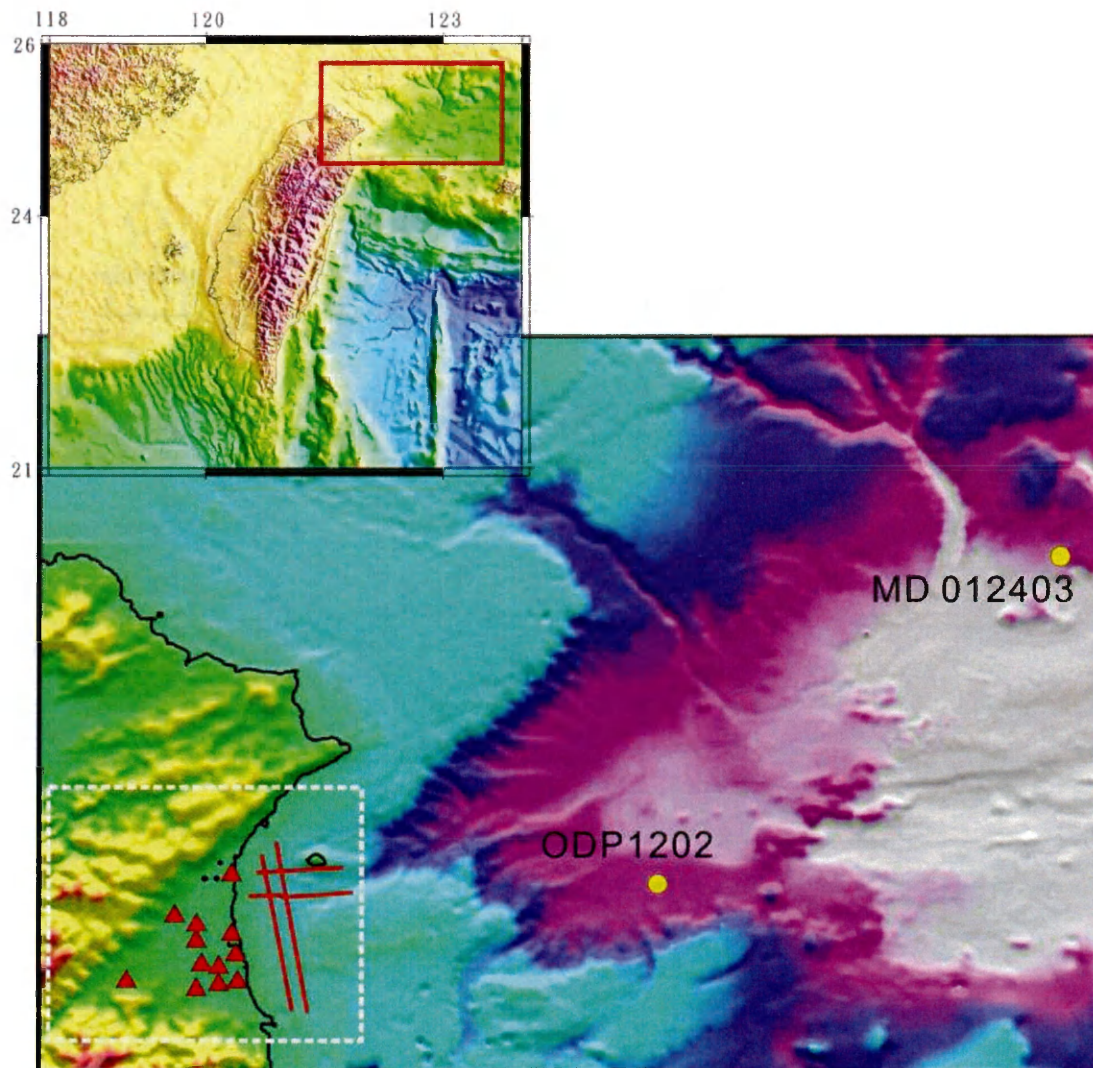
Fig. 5. Locations of core data and seismic survey lines (red lines). The yellow circles with labels are the offshore cores and the red triangular are on-land cores. The white dash square outlines the location of Fig. 6.
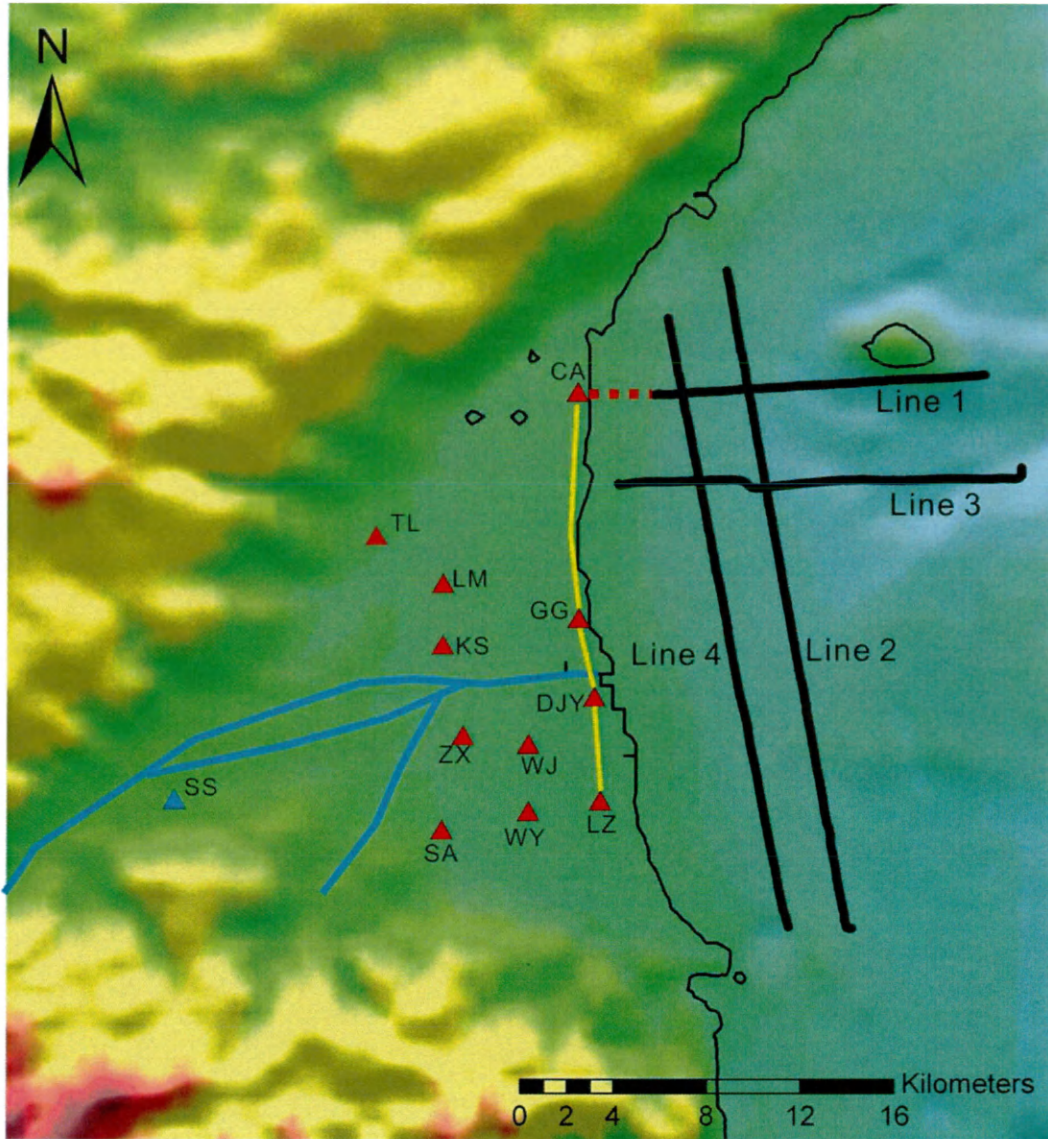
Fig. 6. Detailed location of on-land core sites and seismic survey lines, 4 seismic survey lines are labeled as black colors. The on-land cores with red triangles are used in all the calculations, while the blue one is used in Holocene calculation only. The yellow line represents the location of core correlation in Fig. 10, and the red dash line indicates the gap of core CA and Line 1 in Fig. 15.
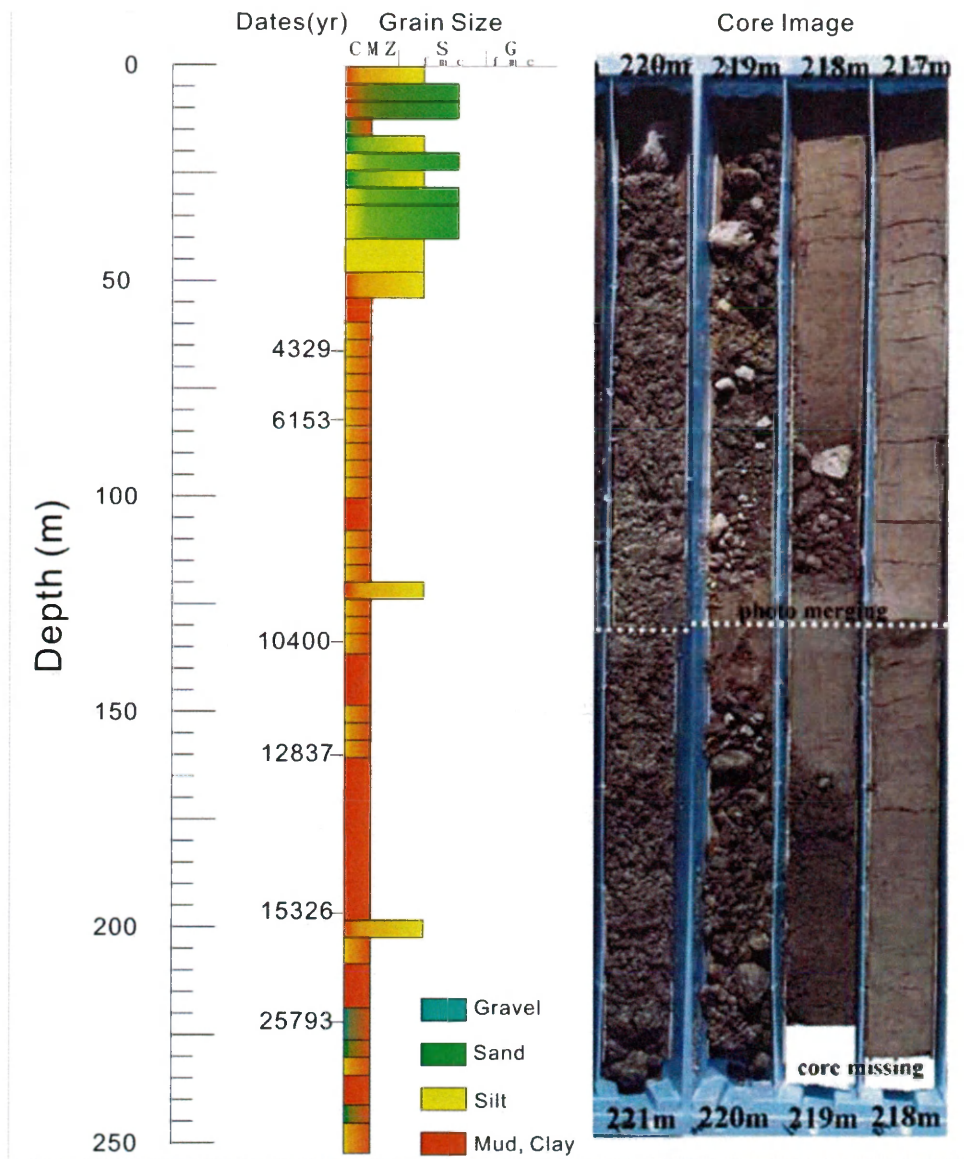
Fig. 7. Example of the core data (core CA). The information includes: core depth, ^{14}C dates, grain size, and a sample of core images with description range from 217m – 221m. The abbreviation letters in the grain size column indicate the grain size index (C =clay, M = Mud, Z = silt, S = sand, G = gravel).
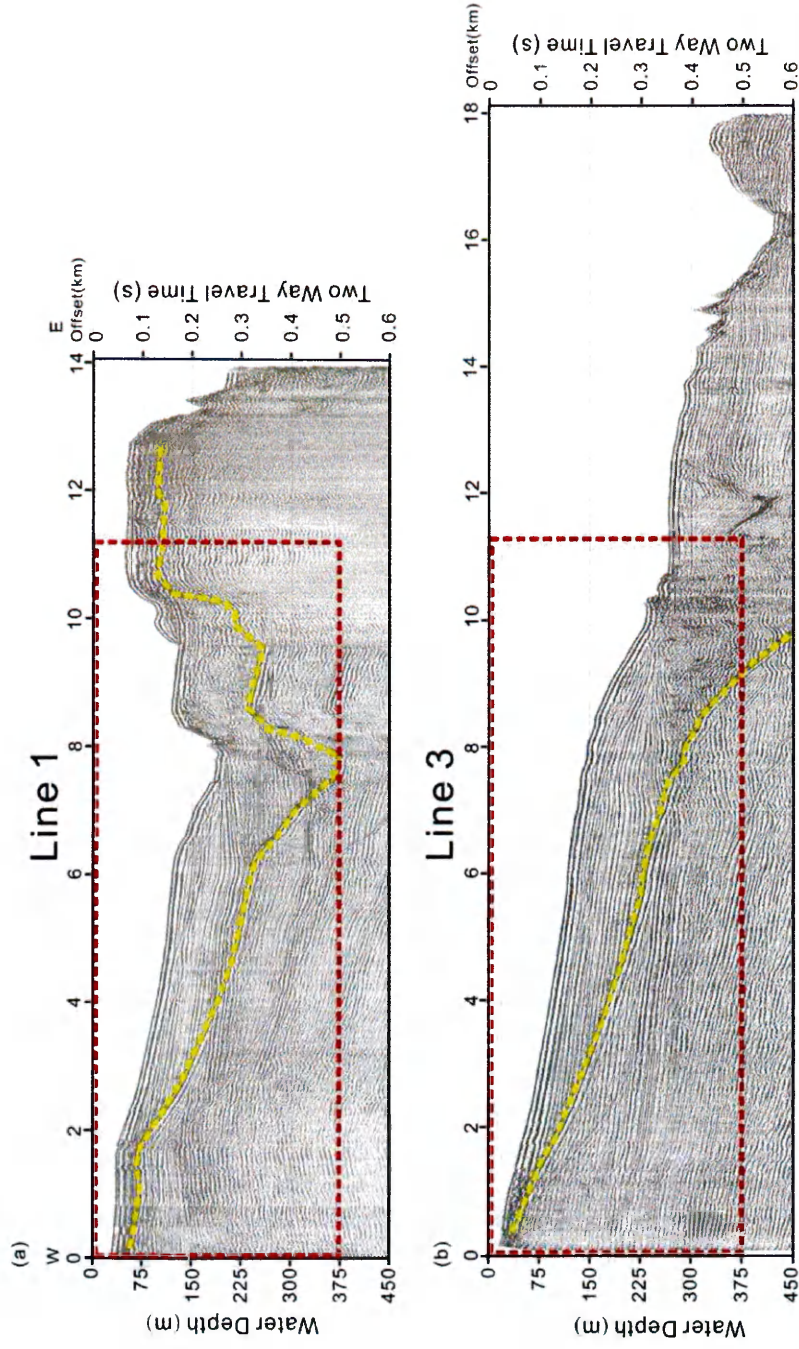
Fig. 8. Two seismic profiles in W-E direction: Line 1(a) and 3 (b).The red dash boxes are the zoom in areas in Fig. 15 and 16. The yellow lines represent the identified multiples in the profiles.

20
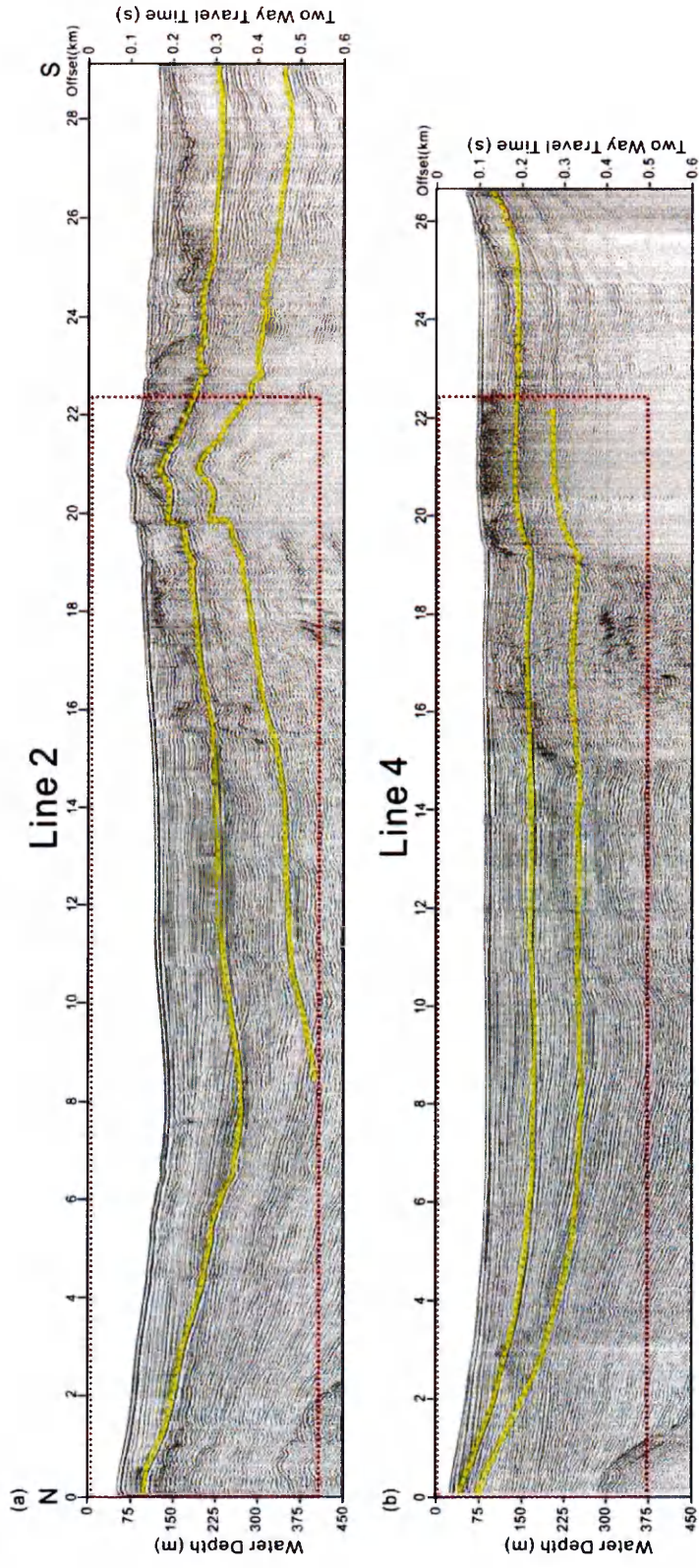
Fig. 9. Two seismic profiles N-S direction: Line 2 (a) and 4 (b). The red dash boxes are the zoom in areas in Fig. 17. The yellow lines represent the identified multiples in the profiles

21

4. Results

4.1. On-land Holocene sedimentation patterns

The on-land dates provide sufficient data to calculate both spatial and temporal variations in sediment accumulation rates, and to identify the approximate Holocene (12 ka BP) boundary. A cross section of five cores shows the general infilling sequences (Fig. 10). Interestingly, coarser sediments seem to predominate the top of the cores, whereas finer sediments dominate the lower parts of most cores. The red dash lines in Fig. 10 indicate different boundaries used to establish the sediment isopach map beginning at the early Holocene (12 ka BP). Results in this section include: 1. Holocene (post-12 ka BP) on-land sediment thicknesses and sedimentation rates; 2. Sediment accumulation patterns during three periods, 0-4 ka BP, 4-8 ka BP, 8-12 ka BP.

4.1.1 Holocene sediment rates

Highest sediment accumulation occurred between ~8 and 12 ka BP, with rates ranging between 10 to 25mm/yr (Fig. 11, Table 1). Two outliers are the extremely low value of 3mm/yr (core TL) and the high value of > 81mm/yr (core LM). Sedimentation rates before and after 8-12 ka BP are generally less than 10mm/yr.

The Holocene isopach map (Fig. 12) shows an average sediment thickness on the Lanyang Plain of greater than 100m, with the thickest sequences>215 m. The

sediment depocenter is located nearby the coastal region, thicknesses gradually

decreasing towards the surrounding mountains.

4.1.2 Sediment accumulation throughout Holocene

The on-land dates not only allow us to define the Holocene boundary, but also are

sufficient to delineate temporal variations throughout the Holocene. Dividing the

Holocene into 4000-yr packages, we can see different deposition patterns (Fig. 13). In

the 0-4 ka BP period, sediment thickness thins landward (Fig. 13a), with greatest

thickness of about 90m near the coast, thinning to less than 20m in the center of

Lanyang Plain. Between 4-8 ka BP, in contrast, sediment thickness seems more

equally distributed across the Lanyang Plain (Fig. 13b), deepest sequences reaching

~60m. In contrast, between 8-12 ka BP, the sediment depocenter is located nearer to

the middle of the present Lanyang Plain (Fig. 13c).

4.2 Off-shore sedimentation patterns

4.2.1. Offshore sedimentation rates

Sedimentation rates in the SOT can be defined by 2 long cores, together with 4

seismic profiles from the Shelf. As with the on-land cores, we find particularly high

accumulation rates between 8 and 12 ka BP. In Fig. 14, the selected on-land core

(core SA) shows highest sediment rate around 9- 13 ka BP, whereas ODP1202 core

has high sediment rate between 8-15 ka BP, and MD12403 between 8-12 ka BP.

Sedimentation rates in MD12403 even exceed 30 mm/yr around 10 ka BP.

4.2.2 Seismic profiles

The Holocene boundary age of core CA can be observed at ~ 150m of core depth,

and this core lien directly ~3 km west of the E-W seismic Line 1 (Fig. 15). An

unconformity can be observed in Line 1 at almost the same depth, wedging out at

the self break. We therefore assume that the sediment lying above the seismic

unconformity represents the Holocene sequence. Line 3, which is parallel to Line 1,

shows a similar unconformity at a water depth of ~190m (Fig. 16). The sediment

thickness in both the seismic profiles ranges between 130 and 170m near the coast,

and gradually wedges out at the shelf break.

Tying Lines 1 and 3, with two N-S seismic profiles (Lines 2 and 4) (Fig. 17) shows

that thicknesses in the north range from 100 to 145m (Line 2), and 60 to 165m (Line

4) in the middle of the Ilan shelf, eventually butting up against a tectonic/volcanic

high in the south. Normal faults also can be seen in several of the profiles.

By using the same method, we can identify the possible unconformity at 8 ka BP.

The result is shown as the dash lines in orange color in Figs. 15, 16&17. This

identified layer, combined with the dates from on-land cores at 8-12 ka BP, allows us

to calculate the total sediment volume during this period.

Isopach maps can be created from Kriging interpolation by picking the depths from the four seismic profiles. In combination with the on-land sediment isopach, an isopach map for the entire region can be created (Fig. 18). Due to the lack of offshore ground-truth (i.e. core data), we have used the dashed lines in Fig. 18 to represent assumed sediment thickness on the Ilan shelf. The sediment depocenter is located in near-shore region, thinning landward towards the mountains and seaward towards Guishan Island and the Ilan Ridge; a small channel extends seaward, but the lack of data prevents us from extending our map farther.

4.3 Converting sediment thickness to sediment volume and mass

4.3.1 Holocene sediment load

By multiplying the areas of individual Holocene layers by sediment thickness provided by the isopach map, we can calculate sediment volume. For the on-land Holocene isopach map, we use ArcGIS software to divide the sediment by 1-m thicknesses for the entire 216 layers (maximum Holocene thickness), from which total sediment volume could be calculated:

$$V_{layer} = (h) \cdot (a) \qquad [Eq.1]$$

Where (h) is sediment thickness of each layer, and (a) is the area in each layer. In this study, we set the (h) value to 1m. Total on-land sediment volume is calculated at

25

~ 30 km^3. Using the isopach map in Fig. 18 and the equation 1 where h = 1 m, we

calculate the offshore Holocene sediment volume to be 27 km^3, meaning that total

sediment volume for the onshore and offshore portions of the Ilan Plain/Delta is 57

km^3.

The dry sediment density (ρ_b) can be calculated by the equation (Burdige., 2006):

$$\rho_b = (1 - \varphi)\rho_s \quad \text{(Eq.2)}$$

Where the ρ_s is the density of sediment particle (assumed to be 2.65g/cm^3), and,

φ is the sediment porosity. Because sediments in the Lanyang Plain contain a mixture

of sand, silt, mud and gravel, Ciang et al. (2008) estimated a porosity range of 0.3 to

0.6, meaning that:

$$\rho_b = (1 - 0.3) \cdot 2.65 = 1.9 \text{ g/cm}^3 \quad \text{(Eq.3)}$$

$$\rho_b = (1 - 0.6) \cdot 2.65 = 1.1 \text{ g/cm}^3 \quad \text{(Eq.4)}$$

Multiplying by the volume by the sediment density gives a total Holocene

sediment mass between 63 to 110 Bt. Dividing this value by 12,000 years, gives an

average annual sediment load of about 5.3 -9.5 Mt/yr(million tons/ yr).

4.3.2 Varying sediment flux throughout Holocene

Onshore cores (Fig. 11) show that Holocene sedimentation across the Lanyang

Plain has been uneven. Using equation 1, we see that total accumulation between 0

and 4 ka BP was 8.6 km^3, multiplying the sediment density (1.1 to 1.9 g/cm^3) and

yield the total sediment load is~ 9.5 – 16.3 Bt, meaning the sedimentation accumulation of ~ 2.4 – 4.1 Mt/yr. For the 4-8 ka BP interval, the calculated sediment volume is 9.2 km^3, this would give weight of 10.1 – 17.5 Bt, and thus the annual sediment accumulation rate of 2.5 -4.4 Mt/yr.

For the 8-12 ka BP period, the on-land sediment volume is 12.2 km^3, which is highest among 3 periods; and hence, the total sediment load is 13.4 - 23.2 Bt, giving an average sediment rate of 3.4 – 5.8 Mt/yr. Together with the prominence of a similar abundance of 8-12 ka BP sediment in seismic profiles (Fig. 15, 16, 17) and its apparent thickness in the shelf sediments. The average 8-12 ka BP fluvial sediment volume of the Lanyang Plain and adjacent Ilan Shelf is 20.7 km^3, and therefore a sediment mass of 22.8 to 39.4 BT, which equates to mean annual sediment flux 5.7-9.9 Mt/yr (Table 3).
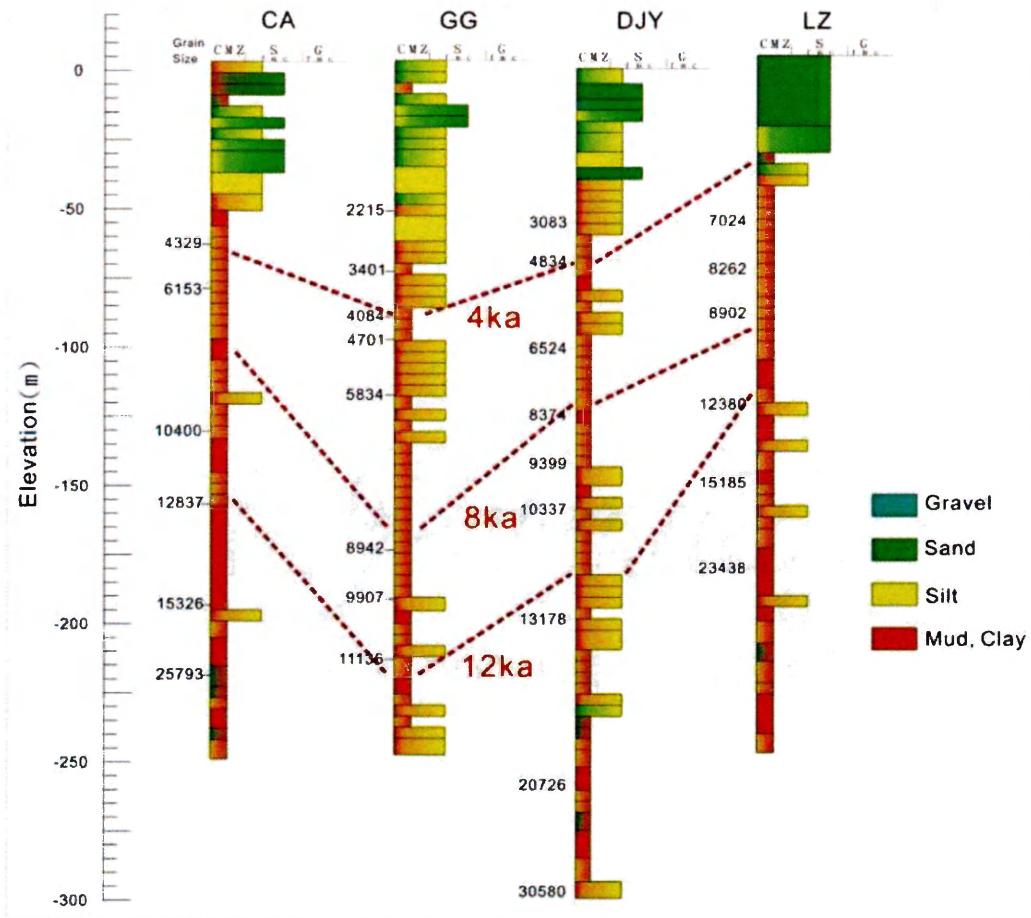
Fig. 10. Sedimentary features and chronological correlation of cores CA, GG, DJY and LZ. The ages in the correlation include 4 ka, 8 ka and 12 ka BP. All ^{14}C dates have been corrected using average calibrated age (Table 2). See Fig. 6 for core locations. The abbreviation letters along the x-axes indicate grain size index (C =clay, M = Mud, Z = silt, S = sand, G = gravel).
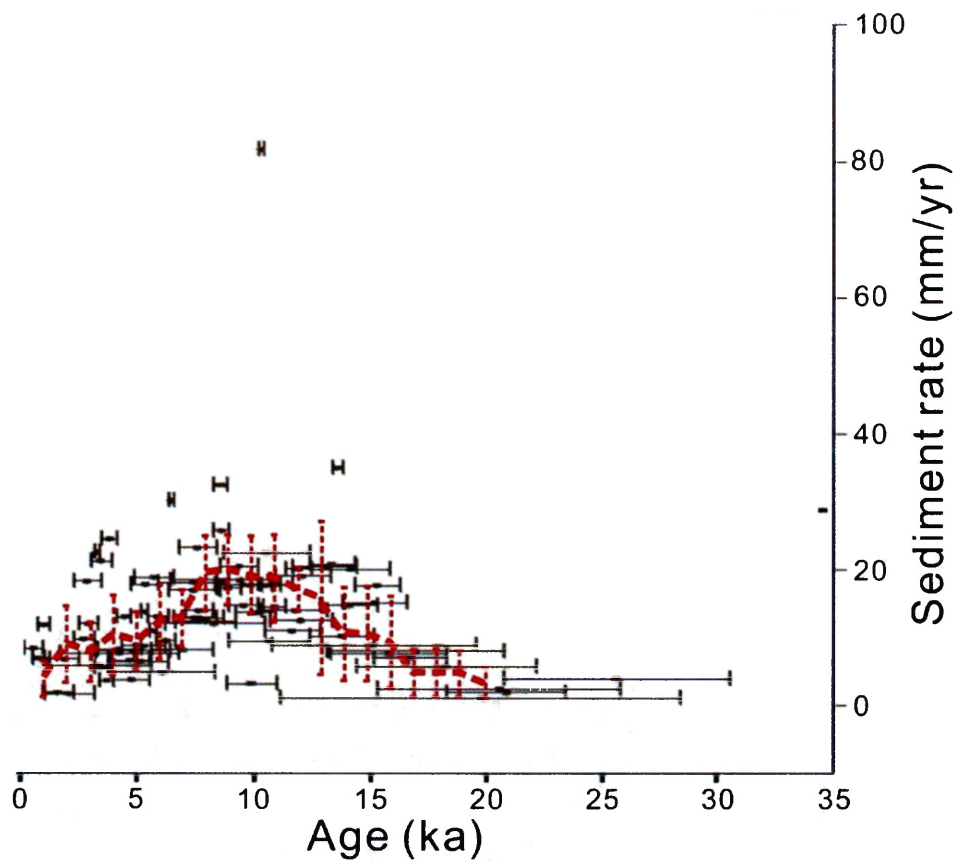
Fig. 11. Relationship between sediment rates and ages of all the on-land cores. The thick red dash line represents the average sediment accumulation rate with the standard deviations in thin red lines. Note the high peak at ~8 ka to 12 ka BP.
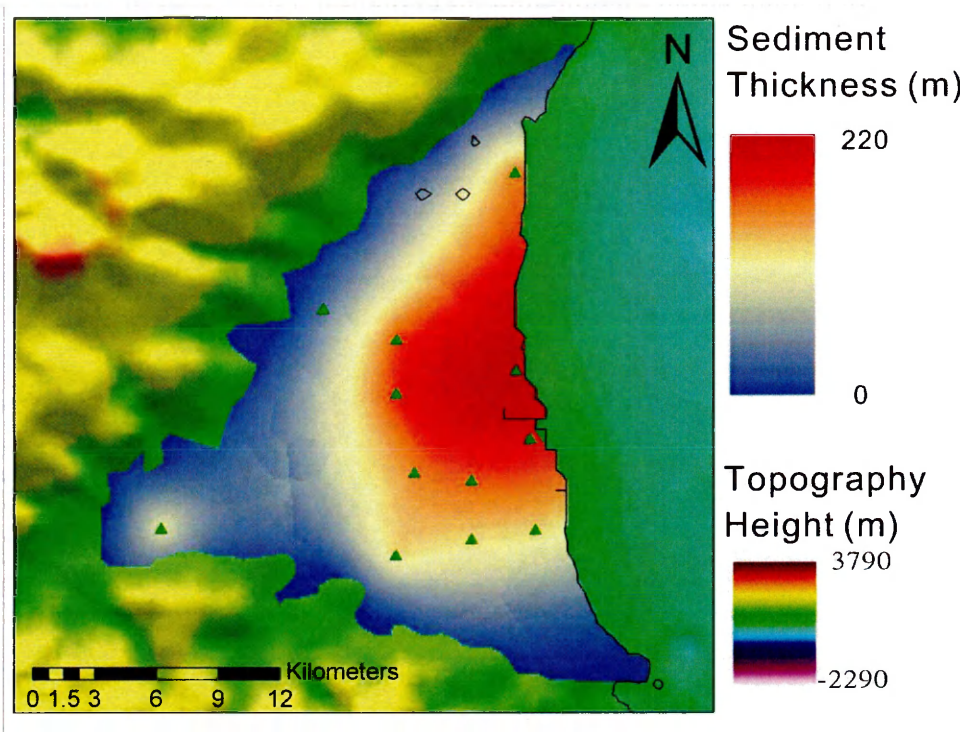
Fig. 12. Post-12 ka sediment thicknesses on the Lanyang Plain. The green triangles represent the core locations.
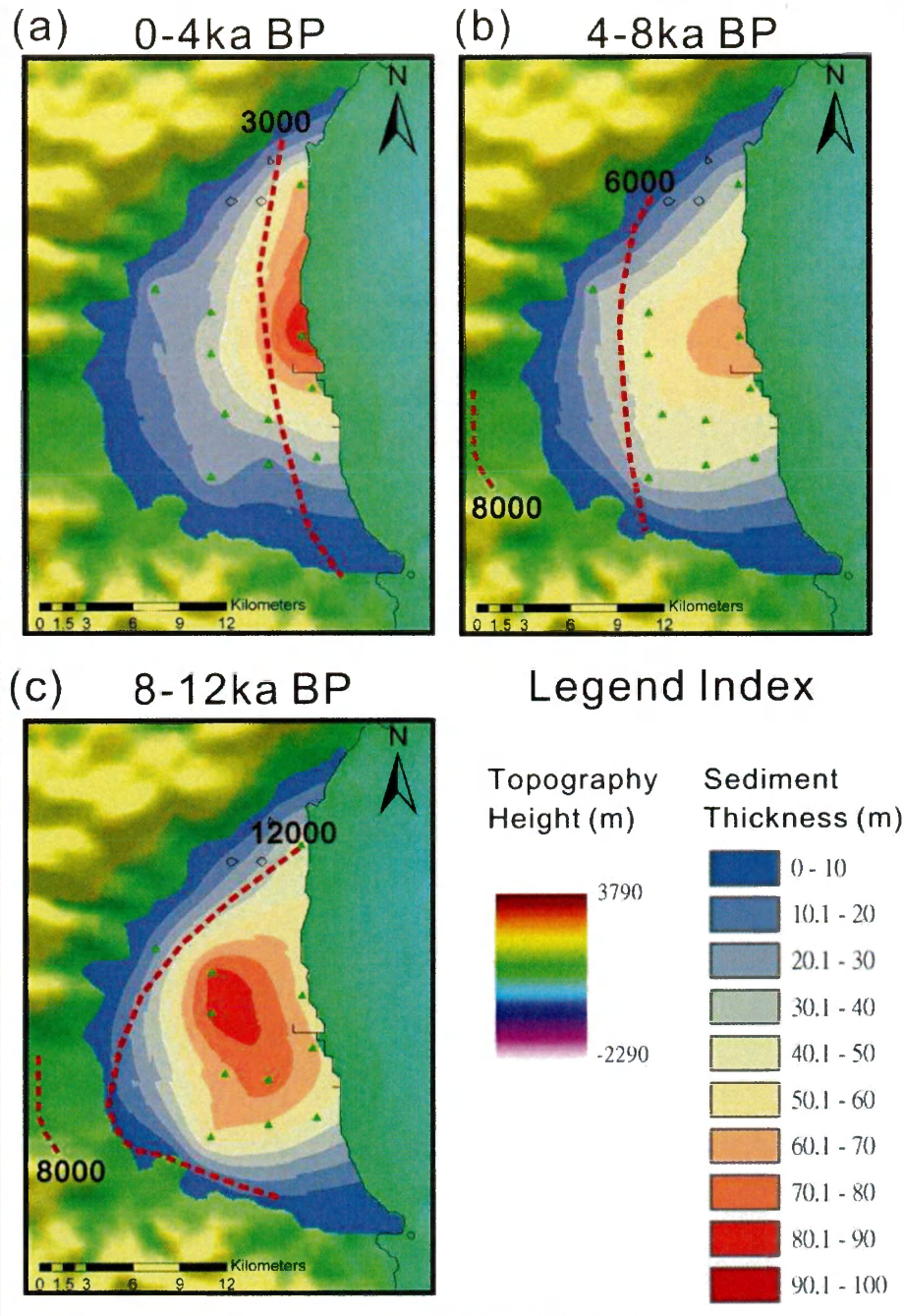
Fig. 13. Sediment distribution during 3 different age-intervals in the Lanyang Plain, 0-4 ka BP(a), 4-8 ka BP(b) and 8-12 ka BP(c). The red lines and ages indicate the locations and ages of ancient coastlines (Chen et al., 2004) and green triangles represent different core locations. The color bars in the right column show the scale of sediment thickness and topography.
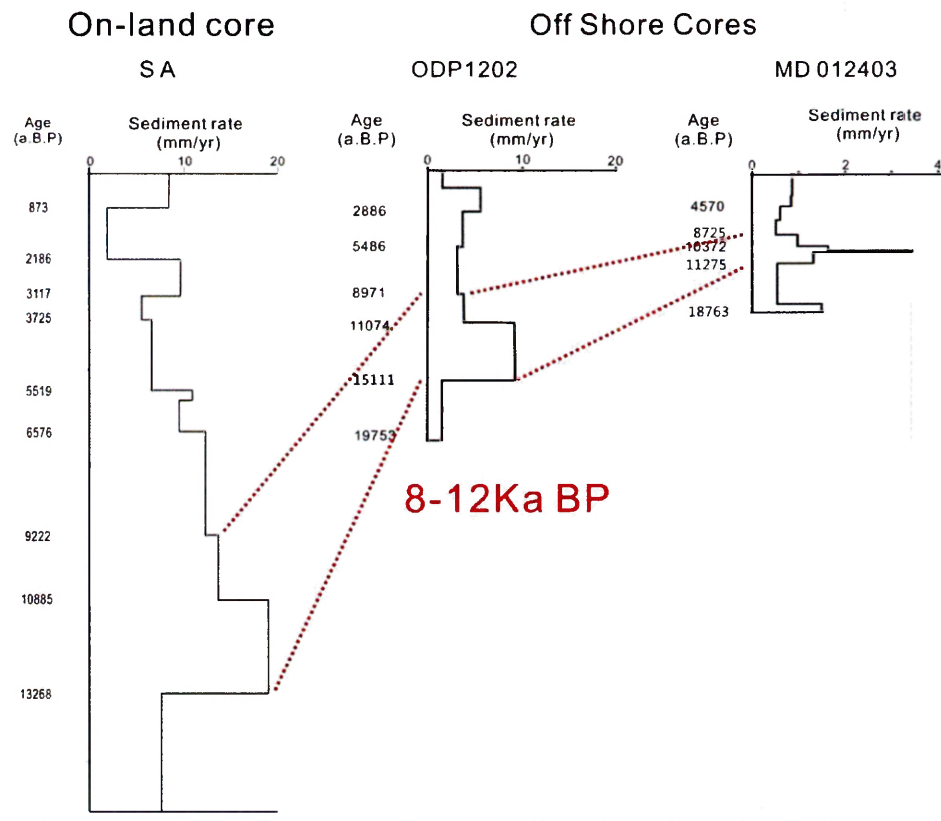
Fig. 14. Sedimentation rates in one on-land core SA and two offshore cores (ODP1202, MD12403). The red dash lines indicate the time period when the sedimentation rate was particularly high, between ~8 and 12 ka BP (see the locations in Fig. 5). Note the X-axis scale of MD12403 is different than the other 2 cores.
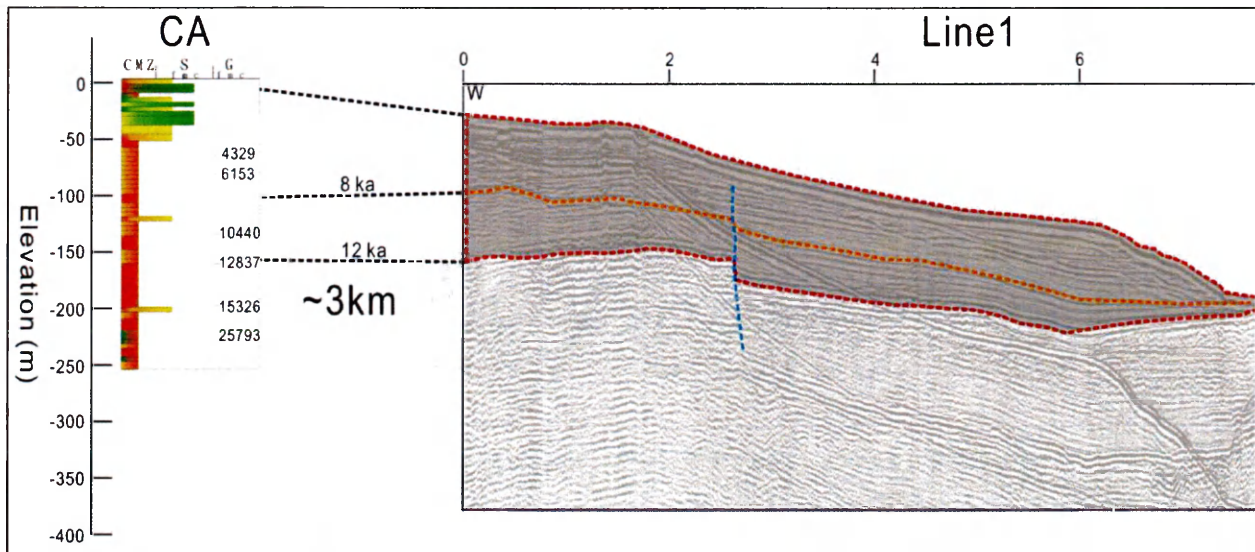
Fig. 15. Seismic profile Line 1 relate to on-land core CA. See Fig. 6 for the core and profile locations. The dist... of Line 1 is about 3 km. The boundary of Holocene in core CA can link to one strong reflection layer, and the surface (surrounded by red dash line) is considered to be the Holocene sediment (layer in grey color). The o... unconformity at 8 ka BP. One significant normal fault present in blue line.
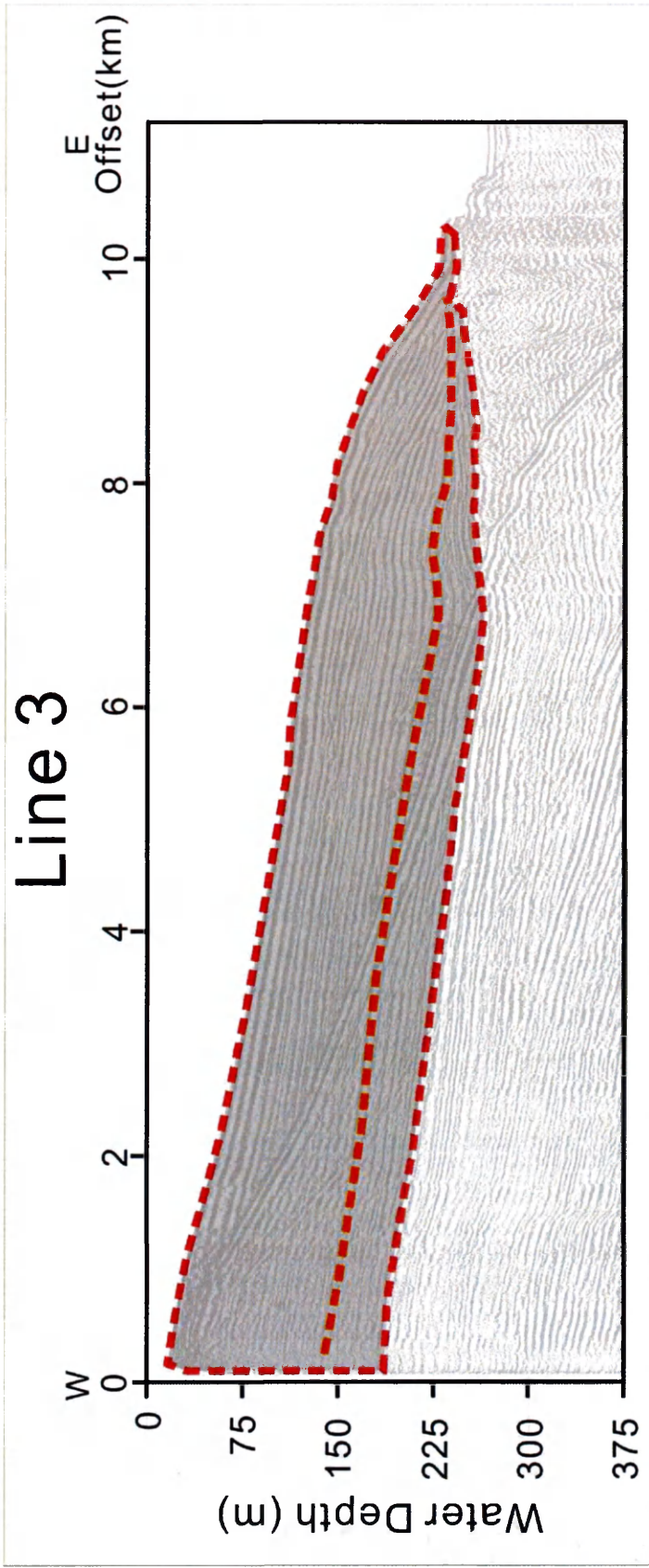
Fig. 16. W-E seismic profile Line 3. All the labels are the same as in Fig. 15. The layer in grey color that surrounded by red dash line is considered to be the Holocene sediment. See Fig. 6 for profile locations.

34
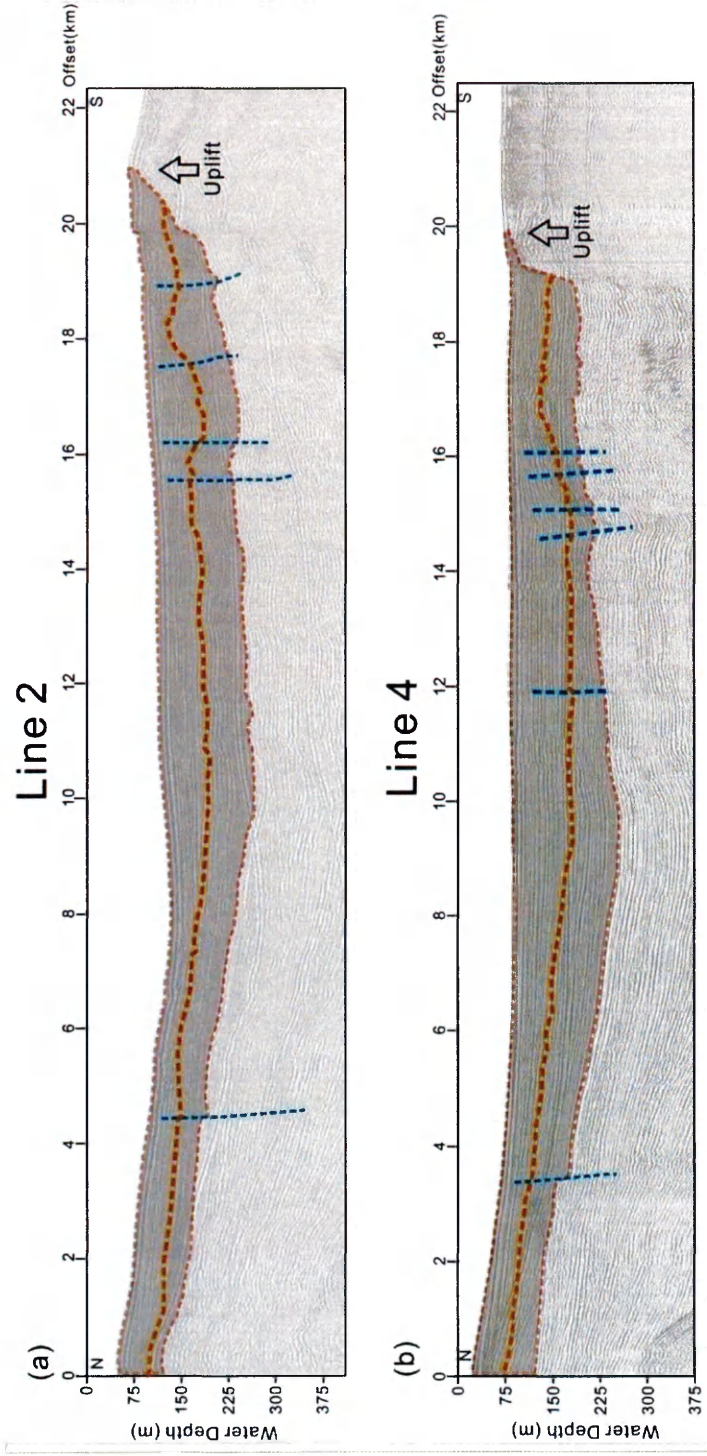
Fig. 17. Two N-S seismic profile, Line2 (a) and Line 4 (b). All the labels are the same as in Fig. 15. Several normal faults (blue lines) are found in the profile of Line 2 and 4. See Fig. 6 for locations of both profiles. The grey areas surrounded by the red lines represent the Holocene sediments. Both profiles end to the south at the Ilan Ridge (see arrows).

35
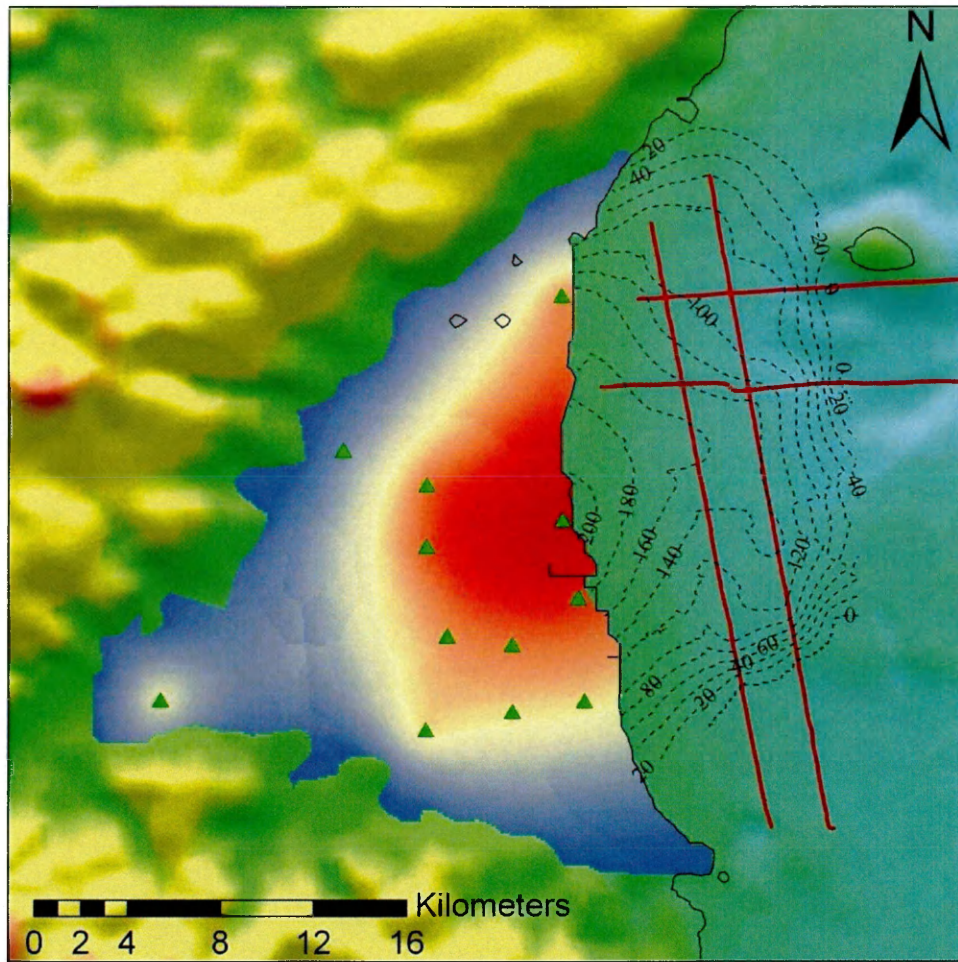
Fig. 18. Post-12 k BP sediment thickness across the subaerial and submarine Lanyang Delta. Because of the tenuous ground-truthing with core CA (see Fig. 6), the submarine isopachs are shown with black dashed lines. Locations of both core (green triangles) and seismic profiles (red lines) are shown. The color scale is the same with Fig. 12.

5. Discussion

5.1 Introduction

Most all the sediment coming to the Lanyang Plain is derived from the Lanyang River and, presumably to a much lesser extent, the mountains bordering the plain. While the Lanyang Plain and adjacent shelf are presumably the primary Holocene sinks, the very high sedimentation rates noted in the offshore cores (Fig. 14) indicate that some of the Lanyang sediment probably escapes to deeper water within the SOT. The >75 m of sediment younger than 15 ka BP at ODP site 1202, for instance, represents one of the thickest post-LGM sedimentary sequences yet sampled by the Ocean Drilling Program.

Thus, while the Lanyang Plain and Ilan Shelf are primary sinks, they do not represent the only site of Holocene sedimentation. Excluding for the time-being the SOT, total Holocene sediment volume on the Lanyang Plain and shelf amounts to ~58 km^3, representing a total mass of 63-110 Bt, equivalent to 5.3-9.2 Mt/yr of sediment flux since 12 ka BP.

On the Lanyang Plain (not included the Ilan shelf), the sediment accumulation rate over the past 8 thousand years has been relatively constant, averaging about 3.4 Mt/yr. However, during the period of 8 - 12 ka BP, the rate was higher, perhaps 3.4 – 5.8 Mt/yr. This is much higher than the sediment rates in other periods.

In a previous study, Kao and Milliman (2008) reported a pre-urbanization (prior to 1958) average annual Lanyang River sediment discharge of 2.6 Mt/yr, about half the calculated Lanyang Plain and shelf Holocene sediment mass. If one considers only the 8-12 ka BP interval for Lanyang Plain and Ilan shelf, sediment discharge from the Lanyang River must have almost reached 10 Mt/yr, which is roughly equivalent to post-1958 Lanyang sediment flux, when road construction and urbanization greatly increased the river's sediment load.

Given the supposition that human impacts on Asian watersheds have resulted in higher (pre-dam) sediment fluxes (Milliman et al., 1987), it is at first disconcerting to realize that early Holocene (8-12 ka BP) sediment loads were as high – or perhaps higher – than seen until road construction in recent years. We can envision two explanations for this:

1) Sediment accumulation rate calculated by Kao and Milliman (2008) was based on the suspended sediment concentration data from WRB (Water Resource Bureau), whose sampling does not measure bedload. This then would mean that actual sediment discharge from the Lanyang may be greater than reported by Kao and Milliman (2008). How much greater is not certain. Kao and Liu (2001) report assume bedload to be 15% of suspended load but admit that periodically it might be much greater.

2) Episodic events (e.g. typhoon, earthquake) can greatly increase sediment load

(e.g., Dadson et al., 2003). In other words, the high sediment loads calculated for the

early Holocene might reflect a period when sediment loads were much greater than

documented before 1958.

We also must consider the post-LGM rise of sea level, which, together with

tectonic subsidence, has provided the space for sediment deposition. According to

previous studies about sea-level changes in Lanyang Plain (Chen et al., 2004), rising

sea level immersed the entire Lanyang Plain from 12 ka to its high stand, about 7.5 ka

BP. Interestingly, this period corresponds with the time when sediment accumulation

rates were the highest. More accommodation space with more on-land sediment

deposition seems reasonable. When the accommodation space is larger, most of the

sediment might be trapped on the on-land region, and yielding the lower sediment

accumulation rate in offshore areas. However, we find more sediment escape from

on-land to far offshore region (Fig. 14) and yield higher sediment rate in SOT during

this period.

This result suggests that during the 8-12 ka BP period, some significant event or

events led to high sediment production and accumulation. The high sediment

accumulation may be related to climatic change – i.e. intensification of the southwest

summer monsoon (Goodbred and Kuehl, 2000) – or to an increase the tectonic

activity (Dadson et al., 2004).

5.2 Possible 8-12 ka BP event

The intense sediment output during 8-12 ka BP documented in this study

suggests a major response of the Lanyang River system to one or more strong forcing

factors. This forcing might be local (e.g., a period of intense earthquakes) or it might

be regional (e. g., climate change). There appears to be no paleo-seismic evidence

that would suggest a greater frequency or magnitude of earthquakes on the Lanyang

Plain and adjacent region during the early Holocene. Alternatively, the genesis of the

higher sediment accumulation may have resulted from the long-term change in

monsoon rainfall. For example, Goodbred and Kuehl (2000) documented particularly

high rates of sediment discharge from the Ganges-Brahmaputra River during the

early Holocene, perhaps in response to post-LGM climate change.

There is, in fact, palynological evidence from the To-she Basin in western Taiwan

(Liew et al., 2006) that suggests the rainfall peaked during the early Holocene (10.7

ka to 8.4 ka BP) (Fig. 19). This early Holocene precipitation optimum has been

interpreted as reflecting maximum intensity of the East Asian summer monsoon

(Hsieh et al., 2011), much the same as suggested by Goodbred and Kuehl (2000).

A broad range of evidence from southeastern Asia indicates the monsoon intensification in the early Holocene. This evidence includes ^{18}O records from stalagmites in China (Wang et al., 2005; Hu et al., 2008) and Arabian Sea ^{18}O records (Sirocko et al., 1993), as well as the pollen record in East Asian region (Van Campo, 1986; Liew et al., 2006) and fossil records in the South China Sea (Huang et al., 1996). This all suggests that the southwest monsoon, which is primarily controlled by the seasonal change of solar insulation, associated with a shift of the inter-tropical convergence zone (Hsieh et al., 2011), may have intensified during the early Holocene, thus providing huge increases in precipitation and heat to East Asia. Such a change in both heat and precipitation could have resulted in an increasing magnitude and/or frequency of typhoons in the Taiwan area.

In addition, large fan-terraces deposited after massive landslides or debris flow events have been noted in both eastern and western Taiwan, having occurred during the early Holocene (Hsieh and Chyi, 2010; Hsieh et al., 2011). In Western Taiwan, Hsieh and Chyi (2010) report a fan–terrace system, Hsin-shung, in the Chen-yeo-lan catchment, which extends for 7 km along the Chen-yeo-lan River, and has thickness as 150 m. This is the largest fan–terrace system in western Taiwan, with dates ranging from 10.8 to 8.9 ka BP (clustering at 9.5–8.9 ka BP) (Hsieh and Chyi, 2010). In Eastern Taiwan, Hsieh et al. (2011) report the Chang-pin/Tu-lan fan terrace, which occupies

more than 6 km^2. Multiple radiocarbon dates range between 11.3 and 8.3 ka BP, with a cluster around 8.6 ka BP. The coincidence in timing of these high sediment output events with the high sedimentation rate seen in the Lanyang Plain and delta supports the concept of a regional climatic forcing. An intensification of the SW (summer) monsoon could have triggered vast rainfall events and perhaps a greater frequency and magnitude of tropical cyclones that collectively led to the 8-12 ka BP sediment flux.
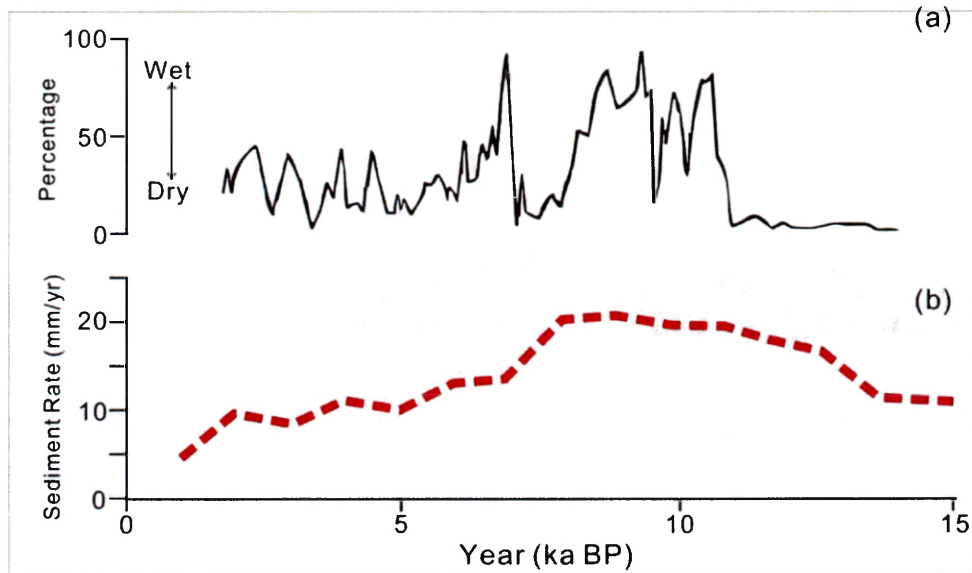
Fig. 19. Comparison between the sediment rates and climate data. (a) is the
summary the spore data from To-she Basin in Western Taiwan (Liew et al., 2006). The
percentage of pollen data could represent different climate conditions (wet or dry).
(b) is the trend of sediment rate variation from on-land cores (extracted from the red
trend line of Fig. 11)

6. Conclusions

1. During Holocene, 57.7 km^3 of sediment have accumulated on the Lanyang

   Plain and shelf; the average sediment accumulation rate is estimated to be

   about 5 -9 Mt/yr in both areas of Lanyang Plain and Ilan shelf. This value is

   higher than the pre-urbanization annual sediment load of 2.6 Mt/yr reported

   by Kao and Milliman (2008).

2. Looking at sediment accumulation rate for various 4000-yr periods on the

   Lanyang Plain, rates during 0-4 ka BP and 4-8 ka BP are about 3.4 Mt/yr on

   the Lanyang Plain. In contrast, the rate of 3.4 - 5.8 Mt/yr between 8-12 ka BP

   is higher. If one includes the sediment that escaped to the SOT, the Lanyang

   during this period must have discharged and enhance the sediment mass in

   SOT. These suggest an event-triggered vast amount of sediment

   accumulation during 8-12 ka BP.

3. The event causing higher sediment accumulation rate during 8- 12 ka BP is

   considered to be the intensification of the southwest summer monsoon in

   Southern Asia region, which might have enhanced the magnitude and/or

   frequency of typhoons impact Taiwan. This event can also be observed in the

   fan-terrace system seen throughout Taiwan (Hsieh and Chyi, 2010; Hsieh et

   al., 2011).

Tables

Table 1. The radiocarbon dates from cores on the Lanyang Plain.

Core name	Materials	Depth (m)	C14 ages (year)	Average calibrated year (BP)	Sedimentation rate (cm/yr)
DJY	C	55.5	2923±42	3083	
	W	69.5	4252±45	4834	0.798
	W	101.2	5722±46	6524	1.876
	W	125.1	7567±52	8374	1.291
	W	142.8	8382±54	9399	1.725
	PI	159.4	9169±58	10337	1.768
	C	198.9	11290±70	13178	1.392
	W	259.1	17512±129	20726	0.797
	S	297.6	26081±412	30580	0.391
ZX	W	24.3	3000±40	3204	
	W	49.4	5570±40	6352	0.797
	W	129.2	9440±70	10687	1.841
	S	162.4	11900±70	13347	1.248
	W	179.4	11960±40	13833	3.494
	W	221.2	13940±50	16606	1.507
WJ	W	19.1	2800±70	2948	
	W	37.7	3530±110	3826	2.120
	W	53.7	5510±40	6336	0.637

	W	90.6	7750±40	8514	1.692
	W	125.1	9090±270	10206	2.044
	S	151.2	10530±40	11673	1.776
	W	206.6	12360±50	14395	2.035
	PI	250.9	18570±80	22175	0.569
GG	PI	54.4	2180±40	2215	
	W	76.1	3170±40	3401	1.830
	W	92.8	3750±40	4084	2.445
	W	100.8	4160±40	4701	1.297
	W	120.9	5100±40	5834	1.775
	PI	176.9	8060±40	8942	1.802
	W	194.7	8810±60	9907	1.844
	W	216.4	9670±40	11136	1.766
	O	223.3	24210±40	28451	0.100
TL	Pe	11.7	1180±49	1079	
	W	37.7	4817±55	5557	0.581
	W	59.8	7428±71	8270	0.813
	W	77.0	7947±73?	8802	3.242
	W	83.8	9614±86	10958	0.315
CA	W	65.9	3900±40	4329	
	S	81.8	5770±60	6153	0.871
	S	133.4	9620±70	10440	1.204

	S	159.7	11250±80	12837	1.097
	W	196.3	12960±50	15326	1.471
	W	221.6	21900±90	25793	0.242
LZ	W	59.7	6110±40	7024	
	W	77.0	7430±40	8262	1.393
	W	93.4	8050±40	8902	2.570
	S	126.0	10860±80	12380	0.937
	S	154.4	13230±90	15185	1.012
	O	175.8	14920±70	18265	0.695
	Pe	185.3	19690±350	23438	0.184
	W	245.5	42855±980		
WY	C	1.8	310±40	388	
	C	5.9	1040±40	982	0.693
	Pl	9.5	2970±40	3133	0.166
	Pl	14.5	3140±50	3355	2.257
	W	16.5	3620±40	3919	0.355
	W	22.5	4740±40	5516	0.376
	W	43.2	3542±55?	3833	-1.230
	W	64.7	7468±71	8287	0.483
	S	108.4	9836±58	10756	1.770
	W	185.9	16410±183	19548	0.882
KS	W	5.22	567±42	616	

	C	11.8	1240±40	1170	1.187
	C	20.2	2340±40	2415	0.675
	W	30.6	3082±54	3282	1.200
	C	45.8	4480±40	5140	0.818
	W	49.3	4669±43	5394	1.381
	C	61.2	5490±40	6305	1.306
	W	68.9	5774±48	6561	3.014
	S	96.2	8158±77	8687	1.284
	W	179.58	10475±63	12411	2.239
	W	218.9	12310±50	14309	2.072
	W	253.7	13658±85	16283	1.762
SA	PI	2.1	112±39	80	
	W	8.8	969±41	873	0.839
	PI	11.2	2170±40	2187	0.187
	PI	20.2	2957±42	3118	0.967
	PI	23.6	3450±40	3725	0.551
	W	35.3	4760±40	5519	0.655
	W	38.2	5032±51	5780	1.092
	W	45.7	5780±40	6576	0.948
	W	78.2	8236±86	9223	1.228
	S	100.9	9954±87	10886	1.365
	PI	146.3	11406±68	13268	1.903
	O	184.8	14990±103	18312	0.764

LM	W	12.1	1760±40	1654	
	PI	51.2	5951±48	6782	0.762
	W	87.8	7540±40	8359	2.320
	W	98.5	8060±40	8942	1.837
	W	116.6	8960±40	10172	1.472
	W	135.2	9250±40	10399	8.176
	W	149.4	9960±40	11377	1.447
	W	171.8	10470±40	12495	2.008
	W	237.9	13310±40	15807	1.996
SS	W	82.8	8160±60	9143	
	PI	102.7	10150±40	11844	0.737
	PI	113.9	13180±40	15618	0.297

1. Location of cores are in Fig. 6.
2. The radiocarbon age were calibrated by using CALIB6.0.
3. BP = Before Present, where present is 1950A.D.
4. Dating material index: C = Charcoal O = Organic mud PI = Plant fracture Pe = Peat S = Shell W= Wood
5. The negative sedimentation rates were labeled as red color, which might indicate the dating age error. Also, the date with material of organic mud were labeled as red color, their values were excluded.

Table 2. The radiocarbon dates from the offshore cores.

Core name	Location	Core Elevation (mbsf)	Depth (cm)	C14 age (year)	Average calibrated year (BP)	Sediment Rate (cm/yr)
ODP 1202	122°30′E	1274	192	1783±45	1295	
	24°48′N		1088	3153±40	2886	0.563
			2048	5135±45	5486	0.369
			3135	8554±70	8971	0.312
			3935	10205±55	11074	0.380
			7735	13340±95	15111	0.941
			8379	17111±70	19753	0.139
			8835	18478±90	21328	0.290
			9635	19810±100	22859	0.523
			10138	20910±120	24998	0.235
			10910	23430±140	27911	0.265
MD012403	123°09.60′E	1420	31	1048 ± 45	588	
	25°16.98′N		241	3244 ± 45	3026	0.086
			371	4432 ± 45	4570	0.084
			491	6164 ± 55	6559	0.060
			601	8211 ± 50	8725	0.051
			761	9553 ± 55	10372	0.097
			951	9557 ± 70	10373	190.000
			1060	10111 ± 55	11040	0.448

			1141	10312 ± 45	11275	0.345
			1351	11325 ± 55	12872	0.131
			1671	15867 ± 65	18763	0.054
			1961	17936 ± 75	20705	0.149
			1991	18000 ± 110	20775	0.429

1. Location of cores are in Fig. 2.

2. The radiocarbon age were calibrated by using CALIB6.0.

3. BP = Before Present, where present is 1950A.D, mbsf = meter below sea level.

4. One of the sedimentation rates were labeled as red color because of its huge value, which might indicate the dating age error.

Table 3. The sediment rate in Holocene (0-12 ka BP) and different periods

Age (ka BP)	Volume (Km^3)	Sediment Load (Bt)	Average Sediment Rate (Mt/yr)
0-4	8.6	16.3 - 9.5	4.1 - 2.4
4-8	9.2	17.5 – 10.1	4.4 - 2.5
8-12 (No shelf)	12.2	23.2 – 13.4	5.8 - 3.4
8-12 (Includes shelf)	20.7	39.4 – 22.8	9.9 - 5.7
0-12 (No shelf)	30.4	57.8 – 33.4	4.8 – 2.8
0-12 (Includes shelf)	57.7	109.6 – 63.5	9.2 – 5.3

Bt = billion ton

Mt = million ton

Reference

Bassinot, F. C., &Baltzer, A., (2002). Scientific report of the WEPAMA cruise, MD122/IMAGES VII, 453 pp. Inst. Fr. pour la Rech. et la Technol. Polaires, Plouzane, France.

Burdige, D. J., (2006). Geochemistry of marine sediments (Vol. 398). Princeton: Princeton University Press.

Chen W. S., (2000). The stratigraphy and deposition environments analysis in the Lanyang Plain. The Bulletin of Central Geological Survey in Taiwan (in Chinese).

Chen, W.S., Sung, S.H., Wu, L.C., Hsu, H.D., Yang, H.C. (2004). Shoreline Changes in the Coastal Plain of Taiwan since Last Glacial Epoch. Bulletin of the Department of Anthropology 62, 40-45 (in Chinese).

Chiang, S.C., (1976). Seismic study in the Lanyang Plain Mining Tech 14, 215-221.(in Chinese).

Chiang H.T., Shyu, C.T., Chang H.I. (2008). A Study of Shallow Geothermal Resources in Ilan Plain, Northeastern Taiwan. Mining & Metallurgy, 52(2), 112-121 (in Chinese).

Dadson, S. J., Hovius, N., Chen, H., Dade, W. B., Hsieh, M. L., Willett, S. D., Hu, J. C., Horng, M. J., Chen, M. C., Stark,C. P., Lague, D., & Lin, J. C., (2003). Links between erosion, runoff variability and seismicity in the Taiwan orogen. Nature, 426(6967),

648-651.

Dadson, S. J., Hovius, N., Chen, H., Dade, W. B., Lin, J. C., Hsu, M. L., Lin, C. W., Chen, T. C., Milliman, J. D.,& Stark, C. P. (2004). Earthquake-triggered increase in sediment delivery from an active mountain belt. Geology, 32(8), 733-736.

Goodbred, S. L., &Kuehl, S. A. (2000). Enormous Ganges-Brahmaputra sediment discharge during strengthened early Holocene monsoon. Geology, 28(12), 1083-1086.

Gourley, J. R., Byrne, T., Chan, Y. C., Wu, F., & Rau, R. J. (2007). Fault geometries illuminated from seismicity in central Taiwan: implications for crustal scale structural boundaries in the northern Central Range. Tectonophysics, 445(3), 168-185.

Hong, E., & Chen, I. S. (2000). Echo characters and sedimentary processes along a rifting continental margin, northeast of Taiwan. Continental Shelf Research, 20(4), 599-617.

Hsieh, M.L., Chyi, S.J. (2010). Late Quaternary mass-wasting records and formation of fan terraces in the Chen-yeo-lan and Lao-nung catchments, central-southern Taiwan. Quaternary Science Reviews 29, 1399–1418.

Hsieh, M. L., Liew, P. M., & Chen, H. W. (2011). Early Holocene catastrophic mass-wasting event and fan-delta development on the Hua-tung coast, eastern Taiwan. Geomorphology, 134(3), 378-393.

Hsieh, M. L., Lai, L. S. H., Lin, C. D. J., & Shyu, J. B. H. (2012). Late Quaternary

landscape evolution and genesis of the 2009 catastrophic landslide in the Hsiao-lin

area, southwestern Taiwan. Geomorphology.

Hu, C.Y., Henderson, G.M., Huang, J.H., Xie, S.C., Sun, Y., Johnson, K.R. (2008).

Quantification of Holocene Asian monsoon rainfall from spatially separated cave

records. Earth and Planetary Science Letters 266, 221–232.

Jeng, W. L., & Kao, S. J. (2002). Lipids in suspended matter from the

human-disturbed Lanyang River, northeastern Taiwan. Environmental Geology, 43(1),

138-144.

Kao, S. J., & Liu, K. K., (2001). Estimating the suspended sediment load by using the

historical hydrometric record from the Lanyang-Hsiwatershed.Terr. Atmos. Ocean. Sci.,

12(2), 401-414.

Kao, S. J., Lee, T., &Milliman, J. D. (2005a). Calculating highly fluctuated suspended

sediment fluxes from mountainous rivers in Taiwan. Terr. Atmos. Ocean. Sci., 16(3),

653.

Kao, S. J., Horng, C. S., Hsu, S. C., Wei, K. Y., Chen, J., & Lin, Y. S. (2005b). Enhanced

deepwater circulation and shift of sedimentary organic matter oxidation pathway in

the Okinawa Trough since the Holocene. Geophysical research letters, 32 (15).

Kao, S. J., Dai, M. H., Wei, K. Y., Blair, N. E., & Lyons, W. B. (2008). Enhanced supply

of fossil organic carbon to the Okinawa Trough since the last deglaciation. Paleoceanography, 23(2), PA2207.

Kao, S. J., &Milliman, J. D. (2008). Water and sediment discharge from small mountainous rivers, Taiwan: The roles of lithology, episodic events, and human activities. The Journal of Geology, 116(5), 431-448.

Lee, C.S., Shorjr, G.G., Bibee, L.D., Lu, R.S., Hilde, T.W.C.(1980). Okinawa Trough: Origin of a back-arc basin. Marine Geology 35, 219-241.

Lee S. Y., (2001).Sediment dynamics off northeastern Taiwan - from fallout nuclides 210Pb, 137Cs, and 239,240Pu. Master thesis, National Taiwan University (in Chinese)

Li, Y. H., (1976) Denudation of Taiwan Island since the Pliocene epoch. Journal of Geology 4: 105–107

Liew, P.M., Huang, S.U., Kuo, C.M., 2006. Pollen stratigraphy, vegetation and environment of the last glacial and Holocene—a record from Toushe Basin, central Taiwan. Quaternary International 147, 16–33.

Liu, C. C. (1995).TheIlan plain and the southwestward extending Okinawa Trough. Jour. Geol. Soc. China, 38, 229-242.

Liu, J. T., Yuan, P. B., & Hung, J. J. (1998). The coastal transition at the mouth of a small mountainous river in Taiwan. Sedimentology, 45(5), 803-816.

Milliman, J. D., & Meade, R. H. (1983). World-wide delivery of river sediment to the oceans. The Journal of Geology, 1-21.

Milliman, J. D., Yun-Shan, Q., Mei-e, R. E. N., & Saito, Y. (1987). Man's influence on the erosion and transport of sediment by Asian rivers: the Yellow River (Huanghe) example. The Journal of Geology, 751-762.

Milliman, J. D., & Syvitski, J. P. (1992). Geomorphic/tectonic control of sediment discharge to the ocean: the importance of small mountainous rivers. The Journal of Geology, 525-544.

Milliman, J. D., & Kao, S. J. (2005). Hyperpycnal discharge of fluvial sediment to the ocean: Impact of Super-Typhoon Herb (1996) on Taiwanese rivers. The Journal of geology, 113(5), 503-516.

Shyu, J. B. H., Sieh, K., Chen, Y. G., & Liu, C. S. (2005). Neotectonic architecture of Taiwan and its implications for future large earthquakes. Journal of Geophysical Research, 110(B8), B08402.

Sibuet, J.C., Deffontaines, B., Hsu, S.K., Thareau, N., Le Formal, J.P., Liu, C.S. (1998). Okinawa Trough backarc basin: Early tectonic and magmatic evolution. Journal of Geophysical Research 103, 30245-30267.

Sirocko, F., Sarnthein, M., and Erlenkeuser, H. (1993). Century-scale events in monsoonal climate over the past 24,000 years: Nature, 364, 322–324.

Stuiver, M., Reimer, P.J., Bard, E., Beck, J.W., Burr, G.S., Hughen, K.A., Kromer, B., McCormac, G., Van der Pflicht, J.,& Spurk, M., (1998). INTCAL98 Radiocarbon age calibration, 24,000–0 cal BP. Radiocarbon 40, 1041–1083.

Suppe, J., 1984. Kinematics of arc-continent collision, flipping of subductionand back-arc spreading near Taiwan. Memoir of the Geological Society of China 6, 21-33.

Syvitski, J. P., Vörösmarty, C. J., Kettner, A. J., & Green, P. (2005). Impact of humans on the flux of terrestrial sediment to the global coastal ocean. Science, 308(5720), 376-380.

Syvitski, J. P., &Milliman, J. D. (2007). Geology, geography, and humans battle for dominance over the delivery of fluvial sediment to the coastal ocean. The Journal of Geology, 115(1), 1-19.

Teng, L. S. (1996). Extensional collapse of the northern Taiwan mountain belt.Geology, 24(10), 949-952.

Tsou, C. Y., Feng, Z. Y., &Chigira, M. (2011). Catastrophic landslide induced by typhoon Morakot, Shiaolin, Taiwan. Geomorphology, 127(3), 166-178.

Van Campo, E. (1986). Monsoon fluctuations in two 20,000-yr B.P. oxygen-isotope/pollen records off southwest India: Quaternary Research, 26, 376–388.

Wang, Y.J., Cheng, H., Edwards, R.L., He, Y.Q., Kong, X.G., An, Z.S., Wu, J.Y., Kelly, M.J., Dykoski, C.A., Li, X.D., (2005). The Holocene Asian monsoon: links to solar

changes and North Atlantic climate. Science 308, 854–857.

Wei, K. Y., Mii, H. S., & Huang, C. Y. (2005). Age model and oxygen isotope
stratigraphy of Site ODP1202 in the southern Okinawa Trough, northwestern Pacific.
Terr. Atmos. Ocean. Sci., 16, 1-17.

Wu, C. H., Chen, S. C., & Chou, H. T. (2011). Geomorphologic characteristics of
catastrophic landslides during typhoon Morakot in the Kaoping Watershed, Taiwan.
Engineering Geology, 123(1), 13-21.

Xu, K., Li, A., Liu, J. P., Milliman, J. D., Yang, Z., Liu, C. S., … &Xu, F. (2012).
Provenance, structure, and formation of the mud wedge along inner continental
shelf of the East China Sea: A synthesis of the Yangtze dispersal system. Marine
Geology, 291, 176-191.

Yu, H.S., Hong, E., 1992. Physiographic Characteristics of the Continental Margin,
Northeast Taiwan.Terrestrial, Atmospheric and Oceanic Sciences 3, 419-434.

Yu, H.S., Song, G.S., 2000. Physiographic and Geologic Frameworks of the
Shelf-Slope Region off Northeastern Taiwan. ActaOceanographicaTaiwanica 38, 1-22.

Vita

Chia-Yu Wu

Born in Taoyuan Taiwan on 2 February 1983. Graduated from Taitung Senior high school, Taitung, Taiwan in June 2001. Earned B.S. in Geoscience Department of National Taiwan University, Taipei, Taiwan in June 2005. Earned the first M.S. with honor in Institute of Oceanography in National Taiwan University. Entered M.S. program in the College of William & Mary, School of Marine Science, Gloucester Point, VA in August 2010.